

K2: Extending Kepler's Power to the Ecliptic

K2 Handbook

KSCI-19116-003

Kenneth Mighell & Jeffrey Van Cleve

24 August 2020

**NASA Ames Research Center
Moffett Field, CA 94035**

Prepared by: Kenneth Mighell Date 8/25/2020
Kenneth J. Mighell, Science Office

Prepared by: Jeffrey E. Van Cleve Date 8/25/2020
Jeffrey E. Van Cleve, Science Office

Approved by: Douglas A. Caldwell Date 8/26/2020
Douglas A. Caldwell, Instrument Scientist

Approved by: Jeffrey L. Coughlin Date 8/25/2020
Jeffrey L. Coughlin, Science Office Director

Approved by: Jessie Dotson Date 8/25/2020
Jessie Dotson, Project Scientist

Document Control

Ownership

This document is part of the Kepler Project Documentation that is controlled by the *Kepler* Project Office, NASA/Ames Research Center, Moffett Field, California.

Control Level

This document will be controlled under KPO @ Ames Configuration Management system. Changes to this document ***shall*** be controlled.

Physical Location

The physical location of this document will be in the KPO @ Ames Data Center.

Distribution Requests

To be placed on the distribution list for additional revisions of this document, please address your request to the *Kepler* Science Office:

Jeffrey L. Coughlin
Kepler Science Office Director
MS 244-30
NASA Ames Research Center
Moffett Field, CA 94035-1000
jeffrey.l.coughlin@nasa.gov

Document Change Log

Change Date	Pages Affected	Changes/Notes
September 18, 2017	All	First release.
July 24, 2019	All	Second release. Includes an updated mission timeline and spacecraft events of note, updated tables and figures, analysis of Kepler characteristic frequencies, updated archive access information, a description of the K2 global uniform reprocessing effort and results to-date, and other minor edits/additions as needed.
August 24, 2020	All	Third release. Structure is significantly re-organized compared to the last release. Includes updated figures and tables after the final data release, additional information on per-campaign observations and data characteristics, including additional figures and data analysis, statistics and information relating to the final data release, and an updated list and description of all data and engineering products available at the NASA archives.

Table of Contents

1. Introduction to K2	7
1.1. Companion Documents	7
1.2. K2 Mission Timeline	8
1.3. Campaign Dates, Cadence Numbers, and Field Positions	10
2. What's New in K2	13
2.1. Spacecraft and Instrument	13
2.1.1. Reaction Wheel Failures	13
2.1.2. Quasi-stable Attitude Control for Ecliptic Fields of View	13
2.1.3. Module Failures	13
2.1.4. Attitude Determination and Control System (ADCS) Modifications	13
2.1.5. Coupling of Low Gain Antenna Operation to Roll Performance	16
2.1.6. Motion-induced Invalid Cosmic Ray Correction	16
2.2. Target Management	17
2.2.1. Overview: Monotony to Diversity	17
2.2.2. Kepler and K2 ID Numbers	18
2.2.3. Extra halos for Stellar Targets	19
2.2.4. Solar System Objects (SSOs)	21
2.2.5. Bright Stars	24
2.2.6. Galaxies	25
2.2.7. Extended Regions of the Sky	25
2.2.8. Reduced Number of Nontarget Science Pixels	25
2.3. Data Processing and Pipeline Updates	25
2.3.1. Major Changes	27
2.3.1.1. Improved Background Correction (Dynaback)	27
2.3.1.2. Better Identification of Good Spacecraft Pointing	28
2.3.1.3. Better Identification of Bad Spacecraft Pointing	29
2.3.1.4. Improved Cosmic-Ray Correction	29
2.3.1.5. Short Cadence Light Curve Production	29
2.3.2. Minor Changes	30
2.3.2.1. LDE Parity Error Flag Ignored	30
2.3.2.2. Momentum Dump Flag Used	31
2.3.2.3. Campaign 13 Bright Star Smear Corrected Properly	32
2.3.2.4. Full Frame Image (FFI) Interpolation Bug Fixed	32
2.3.2.5. Scrambled Uncertainties Bug Fixed	33
2.3.2.6. Target Files Delivered	33
2.3.3. Significant Remaining Processing Issues	33
2.3.3.1. Pixel Mapping Reference File (PMRF) Bug	33
2.3.3.2. Proper Motion Bug	33
2.3.3.3. Sub-Optimal Smear Correction	34
2.4. File Formats	34

3. Evaluation of Performance	36
3.1. Pixel Response Function	36
3.2. Pointing	37
3.3. Photometric Precision and CDPF for Pipeline Light Curves	38
3.4. Data Compression	41
3.5. Fidelity of World Coordinate System (WCS)	41
3.6. Moving Targets	42
3.7. Spurious Frequencies	42
3.7.1 Spurious Frequencies seen in Kepler Data	42
3.7.2 Spurious Frequencies seen in K2 Data	43
4. K2 Data Search and Retrieval	48
4.1. Mission-Produced Data	48
4.1.1 The Ecliptic Planet Input Catalog (EPIC)	48
4.1.2 Raw Cadence Data	48
4.1.3 Calibration Files	48
4.1.4 Target Pixel and Light Curve Files	48
4.1.5 Full Frame Images	49
4.1.6 Engineering Data for Science Campaigns	50
4.1.7 FGS Data for Science Investigations	50
4.1.8 Two-Wheel Concept Engineering Test Data (E2)	51
4.1.9 Driftscan FFIs	51
4.1.10 NExSci K2 Targets Table	51
4.2. Community-Based K2 Science Products	52
4.2.1 MAST HLSPs	52
4.2.2 NExSci Data Tables	52
4.2.2.1 K2 Candidates Table	52
4.2.2.2 K2 Names Table	52
4.2.2.3 K2 ExoFOP	52
References	53
Appendix A. List of Acronyms	55

1. Introduction to K2

The K2 mission began in May 2014 when the *Kepler* spacecraft was repurposed following the failure of the second of *Kepler*'s four reaction wheels in May 2013, which necessitated the end of *Kepler* mission operations. The purpose of this document, the K2 Handbook (K2H), is to describe features of K2 operations, performance, data analysis, and archive products that are common to most K2 campaigns, but different in degree or kind from the corresponding features of the *Kepler* mission. Section 1 provides an overview of K2 operations and resources. Section 2 details differences from *Kepler* in observing, data processing, and file formats. Section 3 evaluates the performance of K2 and the resulting data quality. Section 4 contains information on all available K2 data and where to obtain it.

1.1. Companion Documents

The K2H is meant to be read with the companion documents listed below. They are retrievable from the K2 documentation page (<http://dx.doi.org/10.17909/t9-2btd-va80>) at the Mikulski Archive for Space Telescopes (MAST) at the Space Telescope Science Institute (STScI).

- The Kepler Instrument Handbook or “KIH” (Van Cleve & Caldwell 2016; KSCI-19033-002) provides information about the design, performance, and operational constraints of the instrument, and an overview of the types of pixel data that are available. With the exception of failed reaction wheels and CCD modules, the flight hardware for the K2 mission is the same as that for *Kepler*, although the performance is different.
- The Kepler Data Processing Handbook or “KDPH” (Jenkins et al. 2020; KSCI-19081-003). The KDPH describes how pixels downlinked from the spacecraft are converted by the Kepler Data Processing Pipeline (henceforth just “the pipeline”) into the data products delivered to MAST.
- The MAST Kepler Archive Manual or “MKAM” (Mullally 2020). The MKAM describes the format and content of the data products, and also how to search for them.
- The Kepler Data Characteristics Handbook or “KDCH” (Van Cleve et al. 2016; KSCI-19040-005). The KDCH describes recurring non-astrophysical features of the *Kepler* data due to instrumental signatures, spacecraft events, or solar activity, and explains how these characteristics are handled by the final *Kepler* pipeline.
- The Ecliptic Plane Input Catalog (EPIC) document or “EPIC doc” (Huber & Bryson 2019; KSCI-19082-21). The EPIC doc describes the provenance of the positions and *Kepler* magnitudes used for target management and aperture photometry. There is also an overview of stellar properties (M_{\star} , R_{\star} , T_{\star} , etc.) for K2 targets, with details given in Huber et al. (2016).
- The K2 Data Release Notes or “DRNs” describe each data processing/release, including the delivered data products, their inherent instrumental and astrophysical systematic signatures, and updates to the pipeline software since the last data processing/release. Most DRNs correspond to individual campaigns, and are hosted at MAST (<http://dx.doi.org/10.17909/t9-t116-2c60>).

The KIH, KDPH, and KDCH were updated at the end of the *Kepler* mission and were not revised or reissued to accommodate K2. The EPIC doc was finalized after K2 spacecraft end-of-flight. The MKAM was created at the end of the K2 mission. All K2-specific information is incorporated into the K2H, the K2 DRNs, and the MKAM.

Several published papers provide more thorough treatments of K2 flight operations (McCalmont et al., 2015), data analysis (Smith et al. 2016), and performance (Howell et al. 2014; Van Cleve et al. 2016) through roughly the first 1.5 years of science operations. The K2H will refer to these papers, but will not substantially reproduce their content. Acronyms used in this document are spelled out in Appendix A.

1.2. K2 Mission Timeline

During the K2 mission, the *Kepler* spacecraft was constrained to point in the orbital plane, which is near the ecliptic (§2.1.2). It rotated ~ 81 degrees every ~ 83 days to observe a new field of view (FOV) for a new observing campaign (denoted C<n> for $n=0$ to 19). *Kepler* was in an Earth-trailing orbit and the distance between the Earth and the spacecraft was over 1 AU when the end of flight was declared. Figure 1 shows the approximate FOV boundaries for C0–C19. Typically, the telescope pointed away from the Earth (the ‘anti-velocity vector’ or ‘-VV’), but some campaigns (C9, C16, C17, and C19) pointed towards the Earth (the ‘positive velocity vector’ or ‘+VV’) in order to enable simultaneous ground-based observations. The stellar density (stars per square degree) was constant throughout the *Kepler* mission, but varied significantly between each K2 campaign (see Figure 2).

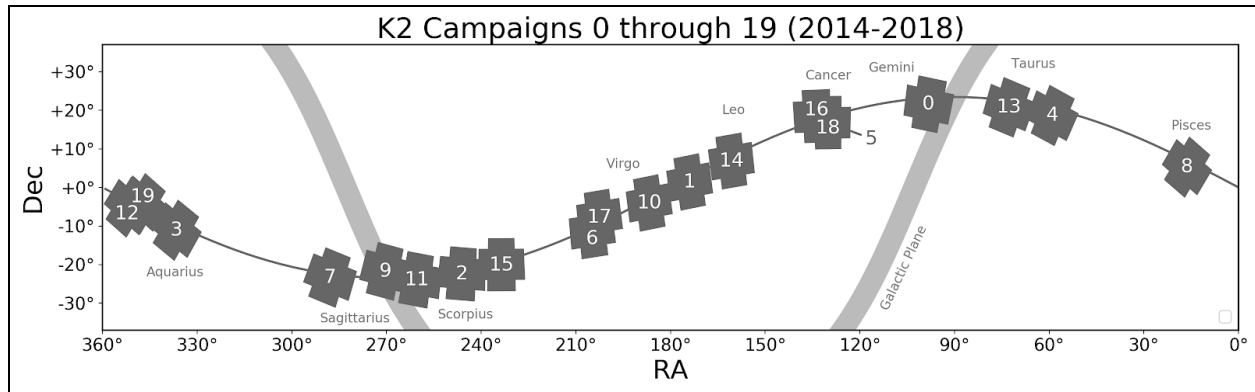


Figure 1: Approximate field of view boundaries for K2 campaigns 0 through 19. The thin line is the ecliptic plane and the thick line is the galactic plane.

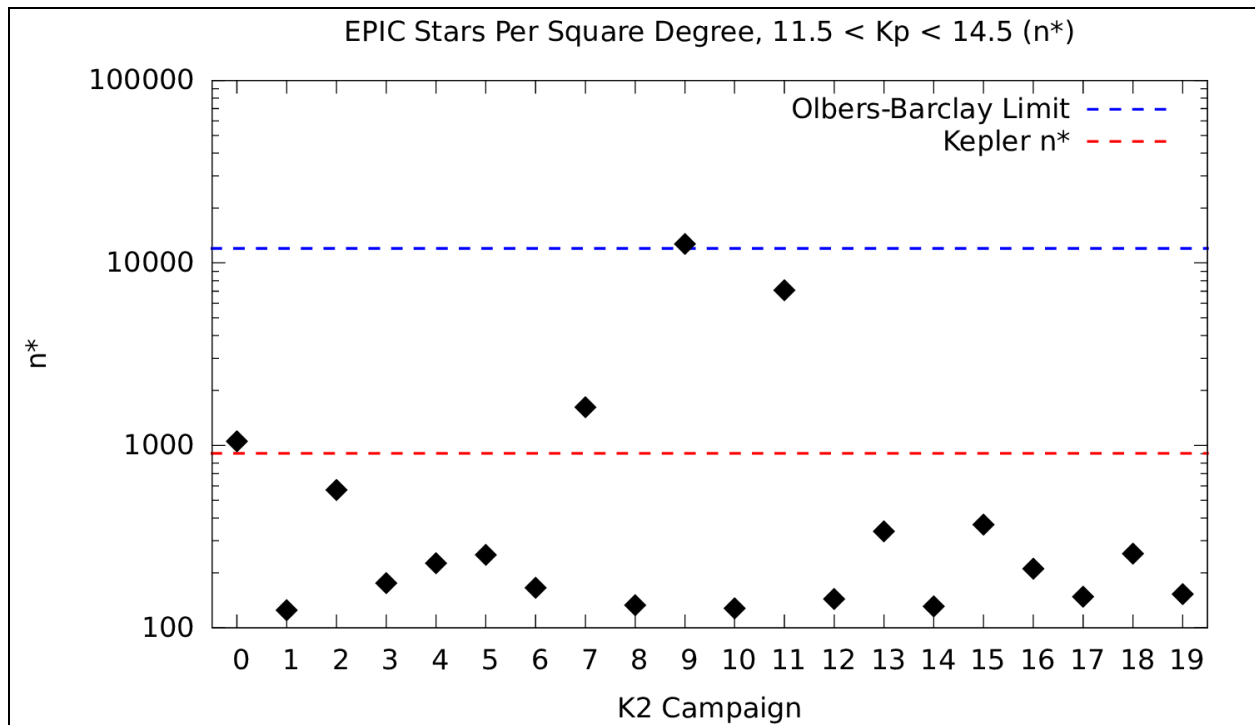


Figure 2: The observed stellar density (n^* ; number of EPIC stars per square degree for $11.5 < K_p < 14.5$ mag) for K2 campaigns 0–19. Also shown for comparison is n^* for the Kepler Field, and the Olbers-Barclay limit. See §3.4 for details, including an explanation of the Olbers-Barclay limit.

The K2 mission experienced the same kinds of science-interrupting events as the Kepler mission, with comparable frequency, and thus the K2 mission timeline (Figure 3) resembles that of Kepler. One new event during K2 operations was a spacecraft Emergency Mode in April 2016, in which the Solid State Recorder (SSR) was powered off — since this occurred between campaigns, no science data were lost.

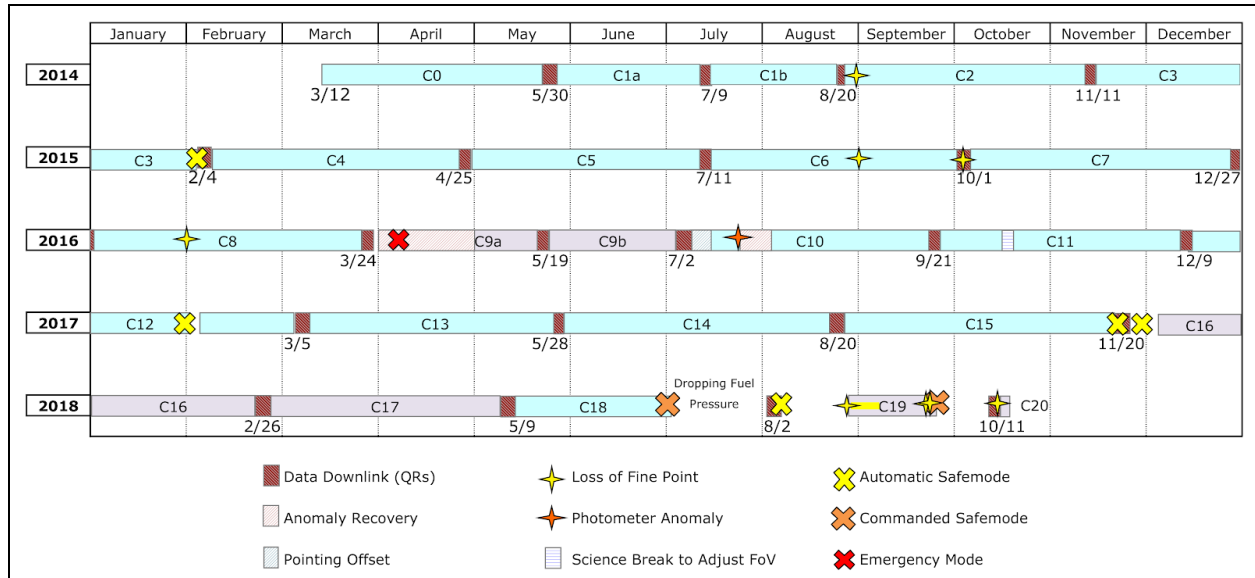


Figure 3: K2 mission timeline showing campaign boundaries and various historical events. The +VV ('positive velocity vector') fields are shown in lavender. While C20 is shown here, no data was collected for it.

The data for C9, C10, and C11 were processed in two parts per campaign, for various reasons. C9 was split to accommodate a larger data volume for this microlensing campaign; most of the target resources were used to tile superapertures (see §2.2.7). C10 had an initial pointing error of more than 3 pixels in boresight. This error was corrected after 6 days; the same set of apertures were used throughout both parts of the campaign since the apertures were designed using the correct pointing. In addition, the correctly-pointed part of C10 is itself split by an unusually long gap during which module 4 failed (see §2.1.3) resulting in a 14-day data gap, though all the correctly-pointed data was processed together. In C11, there was a sign error in the algorithm used to correct for photon pressure emitted by the spacecraft's low-gain antenna (see §2.1.5 for details). The roll angle was corrected and updated apertures were uplinked about 3 weeks after the start of the campaign. While valid data was collected for those three weeks, without the correction and updated apertures, targets at the edge of the focal plane would have rolled out of their apertures by the end of the campaign. C1 and C2 had small pointing adjustments a few days after the start of science, but not large enough to invalidate the photometric apertures. C0 and C1 had mid-campaign breaks, but the data were processed as a single campaign. C19 had complex pointing issues due to low fuel pressure.

Campaigns in which data processing was split into two parts are designated Na/Nb in some contexts and N1/N2 in others, where N is the campaign number. For example, 10b and 102 refer to the same data set. The numerical scheme was chosen for when integer values were required; since C0 and C1 were not split, there is no practical degeneracy in this numerical scheme.

1.3. Campaign Dates, Cadence Numbers, and Field Positions

Cadences (the frequency of observations) are defined in KDCH §1.1. The duration of long and short cadences are the same as they were during the Kepler mission. Table 1 summarizes the start and end times and cadence numbers for each campaign, which may also be found in the individual DRNs.

Table 1: Reference Dates with Cadence Numbers for all K2 Campaigns (C0 – C19).

Campaign	Start Time of First Cadence (UTC)	End Time of Last Cadence (UTC)	LC Start	LC End	SC Start	SC End
0	12-Mar-2014 00:18:30	27-May-2014 16:48:13	87434	91186	2611480	2724069
1	30-May-2014 15:54:44	20-Aug-2014 20:19:37	91332	95353	2728420	2849079
2	23-Aug-2014 18:27:16	10-Nov-2014 13:27:43	95497	99352	2853370	2969049
3	15-Nov-2014 14:06:05	23-Jan-2015 18:37:04	99599	102984	2976430	3078009
4	08-Feb-2015 06:50:09	20-Apr-2015 04:32:47	103744	107213	3100780	3204879
5	27-Apr-2015 02:18:11	10-Jul-2015 22:39:43	107552	111214	3215020	3324909
6	13-Jul-2015 22:45:04	30-Sep-2015 21:11:29	111362	115224	3329320	3445209
7	04-Oct-2015 17:52:39	26-Dec-2015 08:35:28	115414	119456	3450880	3572169
8	04-Jan-2016 13:16:25	23-Mar-2016 06:48:35	119907	123759	3585670	3701259
9a	22-Apr-2016 14:04:59	18-May-2016 22:42:26	125243	126532	3745750	3784449
9b	22-May-2016 14:58:45	02-Jul-2016 22:34:52	126713	128734	3789850	3850509
10a	06-Jul-2016 19:45:29	13-Jul-2016 01:19:55	128925	129230	3856210	3865389
10b*	13-Jul-2016 01:49:21	20-Sep-2016 04:52:03	129231	132614	3865390	3966909
11a	24-Sep-2016 19:12:30	18-Oct-2016 02:16:19	132839	133979	3973630	4007859
11b	21-Oct-2016 06:17:05	07-Dec-2016 23:23:03	134134	136469	4012480	4082559
12	15-Dec-2016 20:40:49	04-Mar-2017 18:37:47	136855	140716	4094110	4209969
13	08-Mar-2017 01:35:06	27-May-2017 15:44:53	140878	144821	4214800	4333119
14	01-Jun-2017 05:06:29	19-Aug-2017 22:11:02	145045	148945	4339810	4456839
15	23-Aug-2017 22:18:11	19-Nov-2017 22:58:27	149142	153449	4462720	4591959
16	07-Dec-2017 23:01:18	25-Feb-2018 12:39:52	154331	158224	4618390	4735209
17	02-Mar-2018 00:33:12	08-May-2018 02:33:28	158445	161727	4741810	4840299
18	13-May-2018 00:44:43	02-Jul-2018 21:51:26	161969	164458	4847530	4922229
19	30-Aug-2018 15:17:06	26-Sep-2018 00:23:59	167333	168623 [†]	5008450	5047179 [†]

*The gap within this data (cadences 129584 and 130268) is due to the failure of module 4 (see §2.1.3).

†The last collected long cadence for C19 was 168624 (and corresponding short cadences 5047180–5047209), but was discarded in processing due to quality issues.

Table 2 shows the K2 campaign field (boresight) positions (right ascension and declination) along with the *Kepler* spacecraft roll angles. The *Kepler* spacecraft coordinates are defined as follows:

- the X axis is the boresight of the *Kepler* photometer (+X points towards the center of the K2 campaign field),
- the Y axis is perpendicular to the solar balance ridge as shown in Figure 4 (+Y points *towards*, but not necessarily directly *at*, the Sun), and
- the +Z axis completes the right-handed orthogonal triad.

During the K2 mission, the Sun was usually kept near the XY-plane (Putnam & Wiemer 2014), which required that the spacecraft be oriented in either the anti-velocity vector (-VV; photometer trailing) or the velocity velocity (+VV; photometer leading) direction. Note that the *Kepler* spacecraft is in an Earth-trailing orbit and aligning the telescope in the anti-velocity direction (done for all campaigns except C9, C16, C17, and C19) prevented stray Earth light from entering the telescope.

The right ascension and declination in Table 2 define the boresight pointing vector (+X) for a K2 campaign and the Roll Angle defines the pointing of the +Y vector; the combination of all 3 values establishes the XY plane that the Sun was either *in* or *near* during normal K2 operations. The nominal R.A. and Dec. positions and Roll Angle values for a K2 campaign are given by the FITS keywords RA_NOM, DEC_NOM, and ROLL_NOM, respectively, in header data unit #1 of each K2 campaign FFI FITS file. The nominal (commanded) roll angle is generally equal to the actual roll angle only near the midpoint of a K2 campaign.

Table 2: Nominal (Commanded) Pointing for each K2 Campaign Field.

Campaign	R.A. (2000.0) (deg)	Dec. (2000.0) (deg)	Roll Angle (deg)
0	98.2985439	21.5904167	177.4754730
1	173.9396100	1.4172989	157.6412060
2	246.1264000	-22.4473000	171.2280000
3	336.6653464	-11.0966638	-158.4948181
4	59.0759116	18.6605794	-167.6992793
5	130.1576478	16.8296140	166.0591297
6	204.8650344	-11.2953585	159.6356000
7	287.8285066	-23.3600182	-172.7803753
8	16.3379975	5.2623459	-157.3538761
9a [†]	270.3544823	-21.7798098	0.4673417
9b [†]	270.3543824	-21.7804700	0.4673417
10a	186.7759491	-4.0259811	157.6277877
10b	186.7794430	-4.0271572	157.6280500
11a	260.3880064	-23.9759578	176.7437075
11b	260.3880064	-23.9759578	176.4237075
12	351.6588124	-5.1023328	-156.8808419
13	72.7971166	20.7870759	-172.7995758
14	160.6824762	6.8509316	158.7573464
15	233.6175730	-20.0792397	166.7780778
16 [†]	133.7099689	18.5253931	-15.0605959
17 [†]	202.5496152	-7.7210759	-20.7870925
18	130.1610170	16.8278629	165.8977388
19 [†]	347.2590265	-4.2027029	22.8818335

[†]Campaigns 9, 16, 17, and 19 were forward-facing campaigns, for which simultaneous observations from the ground were possible throughout the duration of the campaign.

The nominal roll angle can be used to calculate the orientation of the CCD array on the sky. The position angle between “array up” (i.e., the orientation shown in Figure 5) and North on the sky, in the counterclockwise direction, is given by:

$$\text{Position Angle} = \text{Nominal Roll Angle} + 103 \text{ degrees.}$$

The offset of 103 degrees accounts for the orientation between the spacecraft and focal plane assembly coordinates (see Figure 23 of the KIH and references therein). The exact orientation of the array on the sky will very slightly vary about this nominal value over the course of a campaign.

For example, the C18 nominal roll angle is ~165.9 degrees, and thus the position angle is ~268.9 degrees (165.9 + 103). This indicates that North is very nearly along the direction of the vector from the center of the array through the middle of module 15, which is exactly 270 degrees counterclockwise from “array up”.

2. What's New in K2

This section details the differences from *Kepler* in spacecraft performance and operations, target selection and observing, data processing, and data products.

2.1. *Spacecraft and Instrument*

2.1.1. Reaction Wheel Failures

The *Kepler* spacecraft lost the ability to precisely control its attitude while pointing at its target field in Cygnus when the second of four reaction wheels failed in May 2013 (KDCH §4.7), leading to the qualitatively different attitude control and FOV scheme for the K2 mission.

2.1.2. Quasi-stable Attitude Control for Ecliptic Fields of View

The engineering solution to the loss of full 3-axis control is described in detail in McCalmont et al. (2015), Peterson et al. (2015), and Putnam, Gravseth, & Wiemer (2016), and discussed colloquially in Van Cleve et al. (2016). Briefly, since solar radiation pressure was the main perturbing torque and the spacecraft is (mostly) symmetric around the solar panel ridge, the roll axis is in unstable equilibrium when the boresight is pointed in the orbital plane (approximately the ecliptic plane). Residual torques then cause the spacecraft to roll. Figure 4 graphically illustrates this engineering solution (Van Cleve et al. 2016).

During the K2 mission, the *Kepler* spacecraft kept accurate pointing in its orbital plane using solar photon pressure. Immediately after every 12th long-cadence exposure was complete (~6 hours), the spacecraft would autonomously decide if a very brief firing (typically 20 to 100 milliseconds) of the spacecraft thrusters was needed to restore pointing accuracy. The thruster firing flags (see MKAM Table 2-3) indicate if the spacecraft thrusters were fired during an observation; the detailed thruster firing history of the spacecraft is given in the high-frequency (250 mHz) telemetry data (parameters ADATERRX, ADATERRY, and ADATERRZ) given in K2 ancillary engineering files (see §4.1.6). The pointing performance of the *Kepler* spacecraft during the K2 mission is described in §3.2. Spurious frequencies found in K2 long- and short-cadence observations, principally as a result of the thruster firings, are described in detail in §3.7.

2.1.3. Module Failures

Module 3 failed during the *Kepler* mission, and module 7 failed between the *Kepler* and K2 missions. Module 4 failed seven days into C10b (about 2016-07-20 07:00 UT). The cause of the module 4 failure is not known, but the sequence of telemetry faults leading up to the failure and the post-recovery behavior of the focal plane are similar to those seen around the failures of module 7 (January 2014) and module 3 (January 2010). Those failures were attributed to a blown fuse in the focal plane local detector electronics (LDE) driver boards, likely due to the failure of a component in the CCD readout chain creating an over-current load. The remaining 18 science modules ran well up till the end of the K2 mission. Figure 5 shows the location of the inoperative modules in the *Kepler* focal plane. See KIH §4 for a detailed description of the detector properties of the *Kepler* photometer.

2.1.4. Attitude Determination and Control System (ADCS) Modifications

Star trackers, Fine Guidance Sensor (FGS) CCDs in the focal plane of *Kepler*, reaction wheels, thrusters, and the Attitude Determination and Control System (ADCS) software worked together to point the spacecraft. Technically they acquired the desired attitude and kept the boresight at the commanded position in the face of solar radiation torques and thermomechanical drift between the spacecraft and photometer components in the course of a campaign. McCalmont et al. (2015) gives a detailed account of how these components had to be modified in the K2 mission in order to restore precise control of the

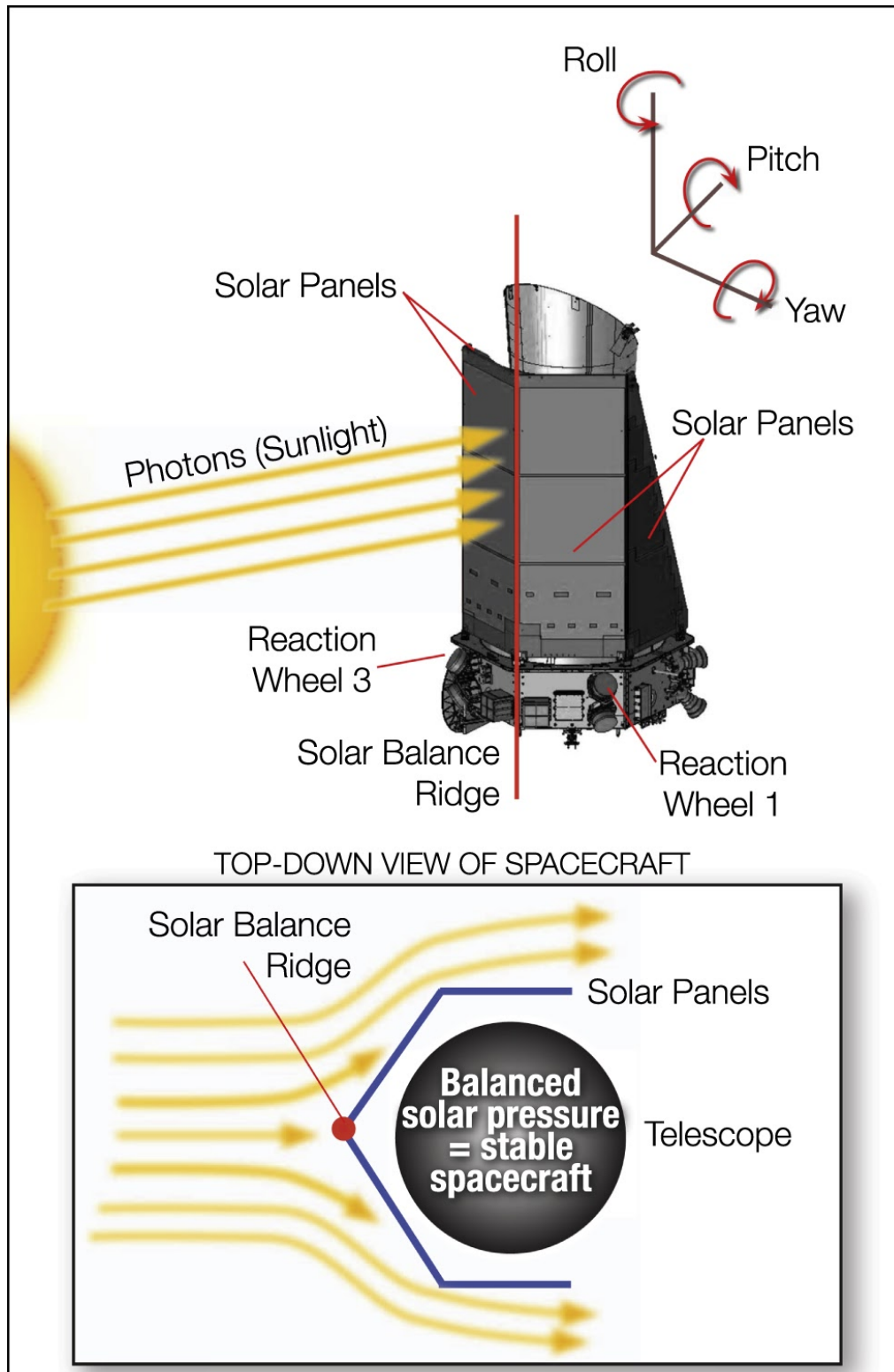


Figure 4: During the K2 mission the *Kepler* spacecraft used its two remaining working reaction wheels (#1 and #3) to point the telescope to a field on the ecliptic plane. The roll axis of *Kepler* is stabilized by the balance of solar radiation pressure and small thruster firings, usually at 6 hour intervals. Figure credit: NASA Ames / W. Stenzel.

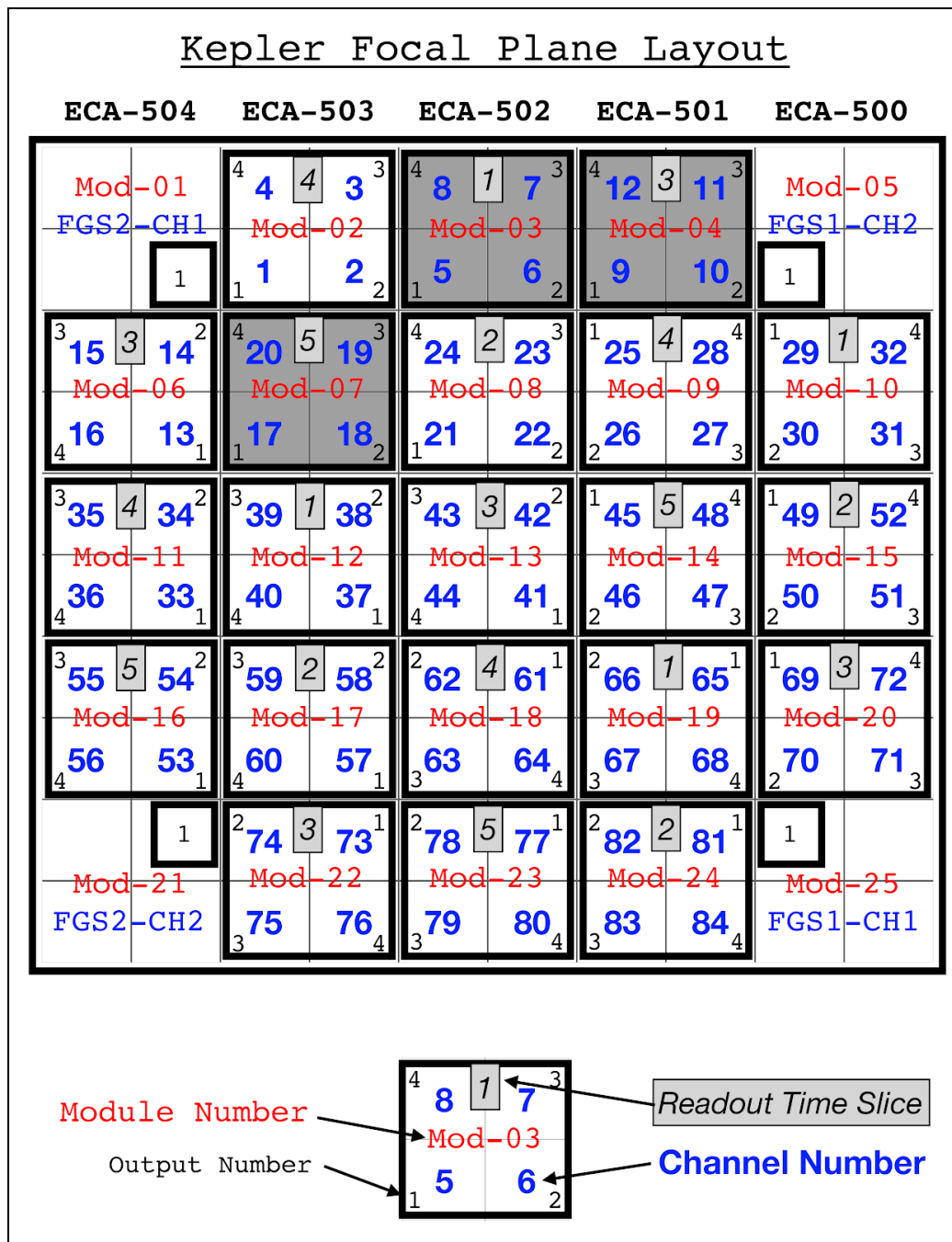


Figure 5: The *Kepler* focal plane layout of modules and CCD channels. There are 21 science modules and 4 Fine Guidance Sensor CCD modules. Each science module is an array of 2200x2048 pixels. Each science pixel has an image scale of 3.98 arcseconds per pixel and a pixel size of 27x27 microns. The 21 science modules each have 4 output channels, for a total of 84 channels and 94.6 million active pixels that view the sky, with additional masked real pixels and virtual pixels for collection of collateral data. By end of flight, three of the modules were no longer in working order (shown as grayed out in the figure) — module 3 failed during Quarter 4 of the *Kepler* mission, module 7 failed between the *Kepler* and *K2* missions, and module 4 failed during Campaign 10 of the *K2* mission.

boresight and acceptable control of spacecraft roll. The changes that most significantly impacted K2 operations and resulting data compared to Kepler were:

- There was only one guide star per module in K2, instead of ten per module as was the case during the Kepler mission. These were carefully screened to exclude variability > 10%, close companions, extended emission, and galaxies. In some fields, suitable guide stars were so sparse that the availability of at least one guide star per module influenced the FOV setting.
- The control bandwidth (ADCS) was increased from 0.02 Hz to 0.05 Hz prior to campaign 3, which greatly improved stability on short-cadence time scales. For the Kepler mission, it was 0.1 Hz.
- The rate at which the spacecraft rolled about the boresight was inversely proportional to the angular momentum and hence wheel speed. The wheels were at their maximum speed immediately after thrusters were fired to unload angular momentum (called “re-sats”).
- There were no longer reaction-wheel zero (speed) crossings (KDCH §5.4).

Throughout the K2 mission, software on-board the spacecraft would record when it considered itself not in fine point. Starting with C14, a change in the on-board software was made to increase the sensitivity in order to better alert spacecraft operators to potential pointing degradation as a result of dwindling fuel supplies. This resulted in additional cadences being flagged as “Spacecraft is not in fine point”, resulting in a needed change to the processing pipeline (see §2.3.1.2).

2.1.5. Coupling of Low Gain Antenna Operation to Roll Performance

Torques generated by the thermal emission of spacecraft equipment – similar to the Yarkovsky-O'Keefe-Radzievskii-Paddack (YORP) effect on asteroids (Rubincam 2000) – were an important part of K2's angular momentum budget. Switching electronics boxes on or off would shift the equilibrium orientation of the spacecraft with respect to that determined in the K2 engineering phase, which assumed default power settings. The most salient example was the switch of Low Gain Antennas (LGAs) in C7 (see the C7 DRN). LGA1 was used for K2 engineering operations and C0–C6, but since the antenna gain is slightly better for LGA2 in the -VV direction, LGA2 was used in C7 to compensate for the ongoing signal loss as the *Kepler* spacecraft gradually drifted away from Earth. C7 showed anomalously high roll error, which was diagnosed as a YORP effect, and the LGA1 was again used starting shortly after the beginning of C8 to restore torques to their expected values. LGA1 was used for the remainder of C8, C9, and C10. The change in roll angle needed to offset the YORP change was calculated and implemented in C11 for LGA2 operations. The calculated sign of the change was unfortunately wrong and the C11 apertures had to be redefined in the middle of the campaign using the correct roll angle. Nominal roll torques with LGA2 operations were achieved for the latter part of C11 and C12–C15 and C18. LGA1 was used for C16, C17, and C19 since they had a +VV orientation.

2.1.6. Motion-induced Invalid Cosmic Ray Correction

The cosmic ray (CR) detection and correction algorithm (KDPH §6.3.1) was developed using the observed characteristics of Kepler data. The design assumes wide-sense stationary data, for which the mean is constant and autocorrelation depends only on the time separation between points. K2 data is not wide-sense stationary, since autocorrelation is time dependent (i.e., correlation between data points separated by a fixed time interval changes with absolute time due to roll cycle). Roughly speaking, motion-induced changes in flux on a given pixel can be mistaken for signal discontinuities produced by cosmic rays. This was recognized early in the K2 mission, and CR detection and correction were turned off for target pixels for all of K2. However, CR detection was enabled for the collateral data (see KIH §2.6.3), which generated many false positive detections in the smear and virtual smear (see KIH §4.5) as bright star flux shifted between adjacent columns due to spacecraft motion. This generated outliers in the time series of the smear data, which were erroneously identified as cosmic rays. When these false positive detections were removed from the collateral data, subtracting that collateral data from the science data resulted in spurious vertical bright streaks. Rather than turn off CR detection for collateral data, which would lead to a comparable amount of error from uncorrected CRs, it was found that an increase in

the CR threshold substantially reduced the number of false positives in the smear and virtual smear, while continuing to do an adequate job of detecting real CRs. This higher threshold was used in C11 and subsequent campaigns, as well as reprocessed campaigns (see §2.3).

CR detection and correction was used on background pixels (pixels not in apertures) throughout the K2 mission, since these apertures were designed not to contain significant stellar flux, and hence are relatively insensitive to image motion induced flux discontinuities.

2.2. Target Management

Target selection in K2 differed significantly from Kepler. This section describes those differences so that users can understand how and why targets were selected, the types of targets observed, and how they were observed, in order to best perform processing of the data and interpret the scientific results.

Due to the complex nature of target management, the following terms are defined up-front for clarity:

- **Target:** An astrophysical object targeted for observation that is covered by one or more apertures.
- **Aperture:** A collection of observed (downloaded) pixels made up of one or more masks.
- **Mask:** A pattern of pixels in a particular shape. Only a finite set of masks (analogous to the finite set of Tetris pieces) can be stored on-board the spacecraft at a given time.

2.2.1. Overview: Monotony to Diversity

The Kepler mission looked at the same field in Cygnus for 4 years. The boresight was fixed, and the spacecraft rotated 90 degrees each quarter. Almost all targets and guide stars were thus simply transferred from one CCD to another for the entire mission. While targets of special interest were added, or especially uninteresting stars were removed, the target list was mostly the same throughout the Kepler mission. Targets were selected before launch from a stable Kepler Input Catalog (KIC), except for a small GO (Guest Observer) program. For each standard target, an optimal aperture (OA) was determined by the Create Optimal Aperture (COA) pipeline module to maximize the anticipated signal to noise, given the target's brightness and the location and brightness of neighboring stars. A combination of masks was selected from the available mask set that covered all the OA pixels while minimizing extra pixels. A detailed description of this process can be found in Bryson et al. (2010a, 2010b) and §3 of the KDPH. In addition, a handful of targets were observed utilizing custom apertures, which were specified manually rather than automatically defined by the pipeline.

In contrast, the K2 mission required a new round of target management for every campaign, including selection of a FOV, targets, and aperture pixels corresponding to those targets. The Ecliptic Plane Input Catalog (EPIC) was updated every campaign to include targets in each new FOV (EPIC doc). In addition, K2 included qualitatively new types of targets, such as Solar System Objects (SSOs; see §2.2.4), which were entirely unforeseen when the Kepler mission was designed. Target management algorithms and procedures were modified to accommodate the new types of targets available in the ecliptic, but no corresponding modifications were made to the photometric pipeline.

The strategy adopted to balance the need for code stability with the ever-changing needs of K2 was to have a stable core of pipeline programs for target aperture definitions (i.e., TAD; see KDPH §3) with flexible MATLAB programs to create the input for TAD, examine its outputs, trim the target list to fit the pixel budget given the estimated on-board data compression (see §3.4), and create summary reports for evaluation and approval.

While no two K2 campaigns were exactly the same, the workflow generally followed this order:

1. The FOV was finalized after rough consideration of science targets and detailed consideration of the availability of FGS guide stars. While the RA and DEC of the FOV center was constrained to be in the ecliptic, and the roll angle was set by the stability requirement, the FOV center could be shifted in ecliptic longitude to maximize a science merit function while having at least one suitable guide star on each FOV module.
2. The EPIC was updated and science targets were selected through the GO proposal process.
3. The GO Office delivered standard target lists, galaxy radii, bright stars with custom circular apertures, SSOs, and overrides to catalog values for proper motion and magnitude. The standard targets are targets for which TAD defined the aperture, and included both stars and galaxies.
4. Masks and apertures were designed for custom apertures (see §2.2.4 – §2.2.6). The set of pixels requested for a single astrophysical target were sometimes broken down into multiple smaller apertures, each of which had a custom EPIC ID assigned to it.
5. TAD was run to define apertures and masks for normal targets (a.k.a. non-custom apertures/targets) like stars and small galaxies. Due to the small (finite) number of masks available, this meant that some targets — especially bright targets — had extra pixels assigned beyond what was needed to optimally capture the flux.
6. On-board data compression estimates (§3.4) yielded the number of LC and SC pixels available.
7. The LC and SC target lists with TAD-defined apertures were trimmed to meet the pixel budget, and the final TAD-defined apertures calculated. In rare instances, custom apertures were removed.

2.2.2. Kepler and K2 ID Numbers

The Kepler and K2 missions used complementary target numbering schemes to label potential targets and observed custom apertures. All the catalogued potential targets in the Kepler field of view were assigned a KIC number. Similarly, all the catalogued potential targets in a K2 field were assigned an EPIC number. When a target was observed using one or more custom apertures during Kepler or K2, a Kepler or K2 ID number was assigned to each aperture. The range of Kepler/K2 IDs assigned to each of these categories is tabulated in Table 3.

Table 3: The Ranges of Kepler and K2 ID Numbers

Kepler/K2 ID Range	Number Type	Catalog	Aperture Type
$< 1 \times 10^8$	Kepler ID	KIC	Standard
$1 \times 10^8 - 2 \times 10^8$	Kepler ID	—	Custom
$2 \times 10^8 - 2.01 \times 10^8$	K2 ID	—	Custom
$> 2.01 \times 10^8$	K2 ID	EPIC	Standard

Targets observed with custom apertures may be associated with multiple Kepler/K2 IDs. For example, K2 observed numerous bright stars with custom apertures (see §2.2.5) — these stars were assigned a K2 ID when the EPIC catalog was generated, and K2 IDs were assigned to the custom apertures used to observe them. Solar system objects (see §2.2.4) and extended regions of the sky (see §2.2.7) were usually observed with multiple custom apertures, each of which was given a K2 ID. For a particular target observed with multiple custom apertures, the assigned K2 IDs are sequential. The K2 search tool or the Custom Aperture File (CAF) at MAST can be used to determine which K2 IDs are associated with a given custom aperture by common name or category. The CAF file for the entire K2 mission (`k2_final_caf.csv`) can be obtained from the MAST archive using a web browser with the following URL <http://dx.doi.org/10.17909/t9-dw50-3e97>.

The number of standard apertures and custom apertures varied from campaign to campaign in order to support the targets selected by the Guest Observer proposal process. Table 4 tabulates the number of standard aperture files, the number of custom aperture files, and the number of total files (standard plus custom) for each campaign for long- and short-cadence light curve and target pixel files, as well as FFIs. Note that the number of light curve files may be less than the number of target pixel files when light curves were unable to be generated for some targets — refer to the campaign's DRN for an explanation in these cases.

The Table 4 column names are defined as follows:

- **llc** is the number of long-cadence light curve files (`ktwo2*_llc.fits`)
- **lpd** is the number of long-cadence target pixel files (`ktwo2*_lpd-targ.fits`)
- **slc** is the number of short-cadence light curve files (`ktwo2*_slc.fits`)
- **spd** is the number of short-cadence target pixel files (`ktwo2*_spd-targ.fits`)
- **ffi** is the number of calibrated full frame image files (`ktwo201*_ffi-cal.fits`)

2.2.3. Extra halos for Stellar Targets

In the Kepler mission, a “halo” of extra pixels was wrapped around the set of OA pixels in order to account for errors in catalog position, proper motion, and the small amount of image motion due to differential velocity aberration (<0.6 pixels) as attitude errors were negligible (KDPH §3). During K2 C0, the roll errors were known to be at least a few pixels, and so conservative halos were used with a width of 10 pixels, which greatly increased the number of pixels per target and therefore significantly decreased the number of targets for which data could be stored. This change of aperture size was particularly severe for fainter stars. For example, the faintest Kepler star has a single-pixel OA giving a target aperture of $4 \times 3 = 12$ pixels, including one-pixel halo and one undershoot (see KIH §6.6) correction column. In C0, the same target would consume $22 \times 21 = 462$ pixels, an increase of a factor of 38!

As K2 progressed, the understanding and control of the flight dynamics improved, and the maximum expected roll motion decreased, so that the number of halo pixels decreased to 6 in C1, 3–4 in C2–C4, and 2–3 in C5–C19. The halos are smaller in the center of the FOV (less than 3.4 degrees from the center) since the roll motion is proportional to the distance from the FOV center for a given spacecraft roll error — an example is shown in Figure 6 using the C18 targets. Thus, for C5–C19, the smallest K2 aperture possible was $6 \times 5 = 30$ pixels in the inner FOV and $8 \times 7 = 56$ pixels in the outer FOV.

The K2 apertures were sized to collect all the pixels that might be in the OA throughout the campaign; in any particular cadence, some of the target pixels may not contain useful source flux. Also note that custom K2 apertures had no halos added.

Table 4: Number of Files per K2 Campaign.

Campaign	Standard Aperture Files				Custom Aperture Files				Total Files				
	llc	lpd	slc	spd	llc	lpd	slc	spd	llc	lpd	slc	spd	ffi
C0	7700	7748	13	13	154	154	0	0	7854	7902	13	13	3
C1	21646	21646	56	56	1	1	0	0	21647	21647	56	56	2
C2	13401	13401	54	54	3264	3264	0	0	16665	16665	54	54	2
C3	16375	16375	55	55	458	458	161	161	16833	16833	216	216	2
C4	15853	15853	122	122	1349	1349	0	0	17202	17202	122	122	2
C5	25137	25137	204	204	637	637	0	0	25774	25774	204	204	2
C6	28289	28289	84	84	19261	19261	0	0	47550	47550	84	84	2
C7	13483	13483	72	72	1602	1602	0	0	15085	15085	72	72	2
C8	24187	24187	54	54	5752	5752	9	9	29939	29939	63	63	2
C9a	0	875	0	11	0	2542	0	1	0	3417	0	12	1
C9b	0	876	0	12	0	2674	0	1	0	3550	0	13	1
C10a	0	28345	0	138	0	13186	0	0	0	41531	0	138	0
C10b	28342	28345	138	138	13186	13186	0	0	41528	41531	138	138	2
C11a	14211	14211	65	65	18601	18601	2	2	32812	32812	67	67	1
C11b	14078	14078	64	64	18430	18430	2	2	32508	32508	66	66	1
C12	29221	29221	141	141	16730	16730	93	93	45951	45951	234	234	2
C13	21434	21434	109	109	4736	4736	9	9	26170	26170	118	118	1
C14	29896	29897	146	147	9129	9129	0	0	39025	39026	146	147	2
C15	23278	23278	118	118	11800	11800	0	0	35078	35078	118	118	1
C16	29888	29888	129	129	5683	5683	2	2	35571	35571	131	131	2
C17	34399	34399	179	179	11831	11831	0	0	46230	46230	179	179	2
C18	20427	20427	235	235	16482	16482	2	2	36909	36909	237	237	1
C19	33863	33863	216	216	10289	10289	6	6	44152	44152	222	222	2

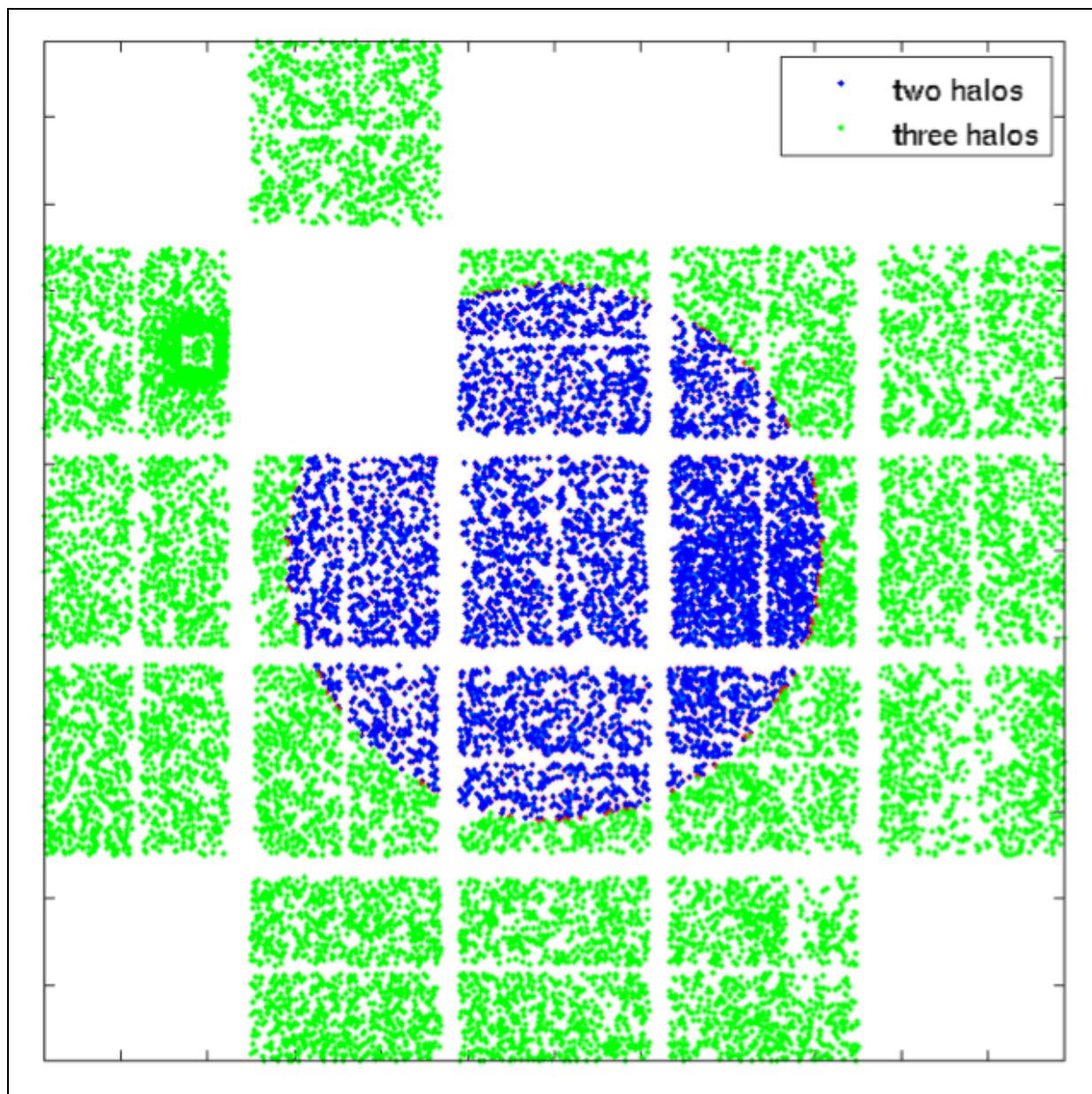


Figure 6: C18 targets plotted on the detector and colored by number of halos added to create their aperture. Core targets (**blue**) had 2-pixel halos while outer targets (**green**) had 3-pixel halos.

2.2.4. Solar System Objects (SSOs)

Kepler was not designed to observe Solar System Objects (SSOs), but these were common targets in K2, including planets (e.g., Uranus and Neptune), moons (e.g., Callisto), comets (e.g., Siding Springs), and asteroids (e.g., Hekate). New strategies were required to observe SSO targets since they move on the sky as seen by K2. In addition, each SSO required a bespoke observing approach. Different SSOs move at different rates and sometimes they traverse multiple photometer channels. The width of the arc of pixels necessary to capture flux from an SSO depended on the objects' brightness. Furthermore, even though an SSO is only observed by a handful of pixels at a time, the custom apertures to collect the SSO flux must be defined for the entire campaign.

Defining a single mask to cover an SSO's entire arc was deemed to be impractical, since the mask would have contained several thousand pixels per arc and would have been good only for that particular SSO. A campaign's mask pixel budget of 87,040 pixels could be quickly exhausted on SSOs alone. Instead SSOs were observed by tiling together masks consisting of a single row (horizontal) or column (vertical) of pixels to cover the arc. SSO arcs could then be composed of a mix of these horizontal and vertical masks. An example is shown in Figure 7.

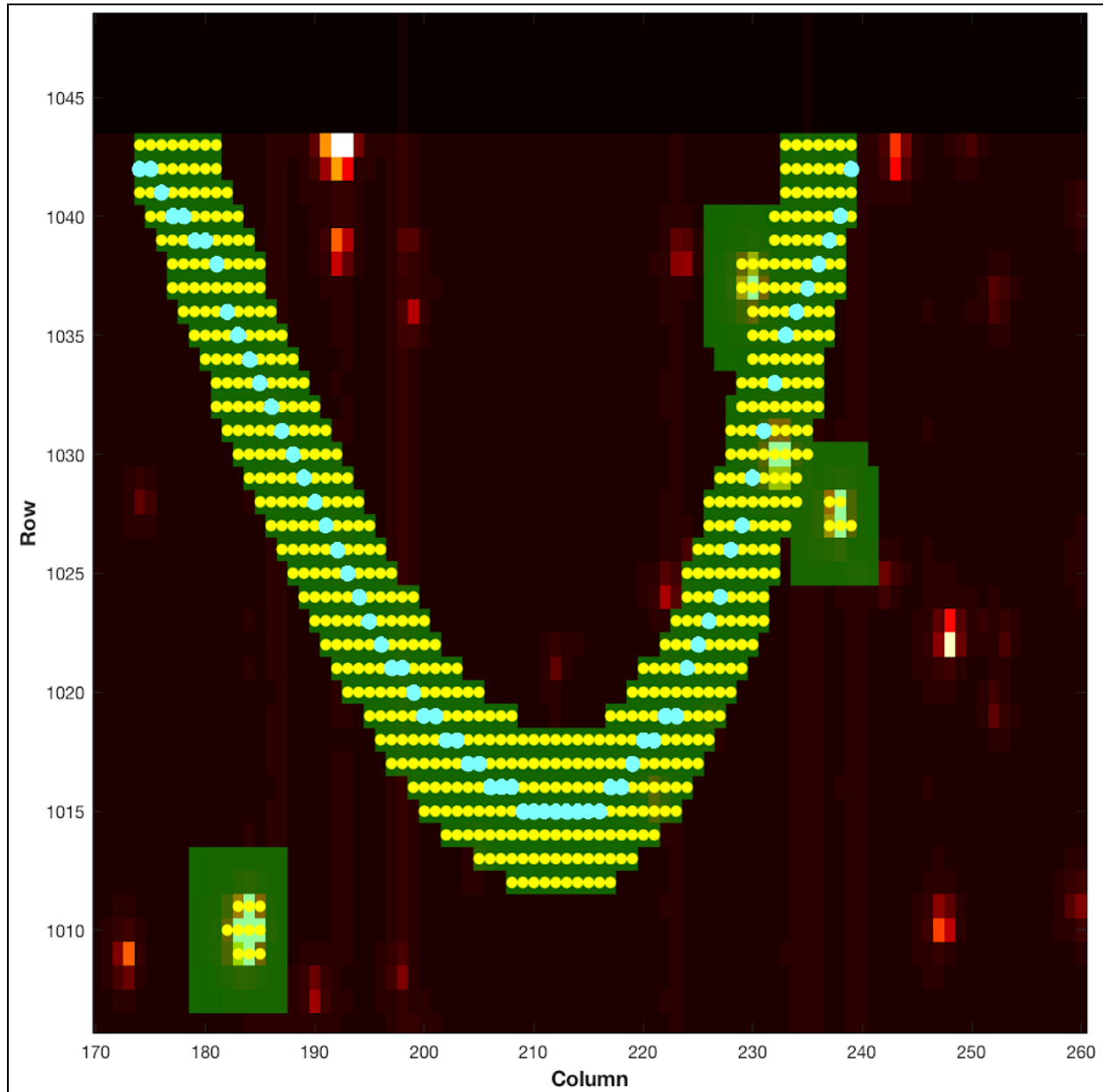


Figure 7: The set of custom apertures for the dim ($K_p \sim 19.8$) SSO 2000_UX34 (a Trojan Asteroid). Blue dots show the center of custom apertures (vertically oriented $1 \times N$ strips) comprising the path of the SSO, with one blue dot per column. Yellow dots (and blue) show the OA pixels, the aperture pixels are colored green, and the stars are colored red/white. Roughly rectangular apertures near the arc that do not have a blue circle are apertures for stellar targets.

The paths in astrometric RA and DEC of all SSOs were computed from JPL Horizons, for which the observer body ID of the *Kepler* spacecraft is -227. K_p was then approximated from the Horizons visual magnitude or from the literature. The SSO path across the detector was then calculated (as shown by the blue circles in Figure 7). Since the OA for stellar sources with $K_p \geq 15$ is a 2x2 box or smaller depending on the pixel response function (PRF) and subpixel registration, for faint SSOs the target pixels were “spraypainted” on the focal plane by convolving the path with a disk that had a default radius of 3.5 pixels (resulting in the yellow dots in Figure 7). This ensured the optimal pixels stayed within the aperture even as the *Kepler* spacecraft rolled. Horizontal and vertical tiles were then assigned to exactly cover the target pixels, with the unique set of masks inserted in the mask table.

For SSOs of intermediate brightness — bright enough to have OA larger than the faint stellar source limit, but not bright enough to bleed charge ($11.5 < K_p < 15$) — the target was treated as a series of instantaneous targets in a special COA run. A maximum width needed to capture sufficient flux was estimated, and a disk of that diameter was convolved with the path, similar to the faint-source procedure. For example, Enceladus ($K_p \sim 12.3$) in C11b had a convolution disk radius of 5 pixels.

For the brightest SSOs ($K_p < 11.5$), the special COA run results were used directly, and a set of vertical or horizontal masks defined to exactly cover all of the OA pixels along the SSO's path. The corresponding unique masks were inserted in the mask table. For example, this was done for Titan ($K_p \sim 8.9$) in C11b.

Use of the tiling scheme for SC SSOs could impose high data volume costs since the SC collateral (SCC) data was individually collected for each target (KIH §2.6.3.2), with no removal of duplications, and the uncompressed data volume of each SCC pixel time series was 30 times that of a LC pixel time series. For long arcs, the preferred scheme was then to cover the SSO's path of OA pixels with a two-dimensional dedicated mask for a small number of targets (instead of one target per row/column). Duplication of SCC data was then reduced, but the mask table had to accommodate a large dedicated mask, consuming mask table pixels that could have been used to more efficiently cover the stellar targets. For example, in C8 the path of Uranus was tiled with 245 single column target definitions at long cadence but with eight 9 x 307 trapezoidal masks (and one small end cap mask) at short cadence. These masks eliminated the redundancy of SCC smear data, but there was still 8x redundancy in the SCC black data.

Later in the mission timeline a bug was found that affected SSO target masks for C0–C15 (and was fixed for C16–C19 target management). Due to a 0- versus 1-based indexing error, all SSO target masks for C0–C15 are displaced by 1 pixel from their optimal positioning. The observed pixels are one pixel to the left and one pixel below their correct positions, in an image orientation with the origin in the lower left, row number as the ordinate, and column number as the abscissa. Note that the object path itself had the correct pixel coordinates — only the selection of pixels for downlink was affected by the bug. An example for Chiron in C12 is shown in Figure 8. Users may also see this offset in movies of the object path (for example, the Pluto movie in the C7 DRN). For compact objects the science impact is expected to be minimal due to the size of each tile, which as mentioned above, was a minimum length of 7 pixels to account for variations due to positioning errors and spacecraft roll. However for extended objects, such as comets, if the PSF wings extend outside of the downloaded apertures it may have a more significant impact.

At the time of this writing, data for a particular SSO may be easily located, either by family or individual names, on the MAST K2 Data Search and Retrieval page by clicking on the “Object Type” link. That page can be accessed by clicking the “Search” link in the Data section on the MAST K2 Search and Retrieval page (<http://dx.doi.org/10.17909/t9-6zdf-eh42>), and/or by searching the CAF file for the entire K2 mission (`k2_final_caf.csv`), which is available for download at MAST (<http://dx.doi.org/10.17909/t9-dw50-3e97>).

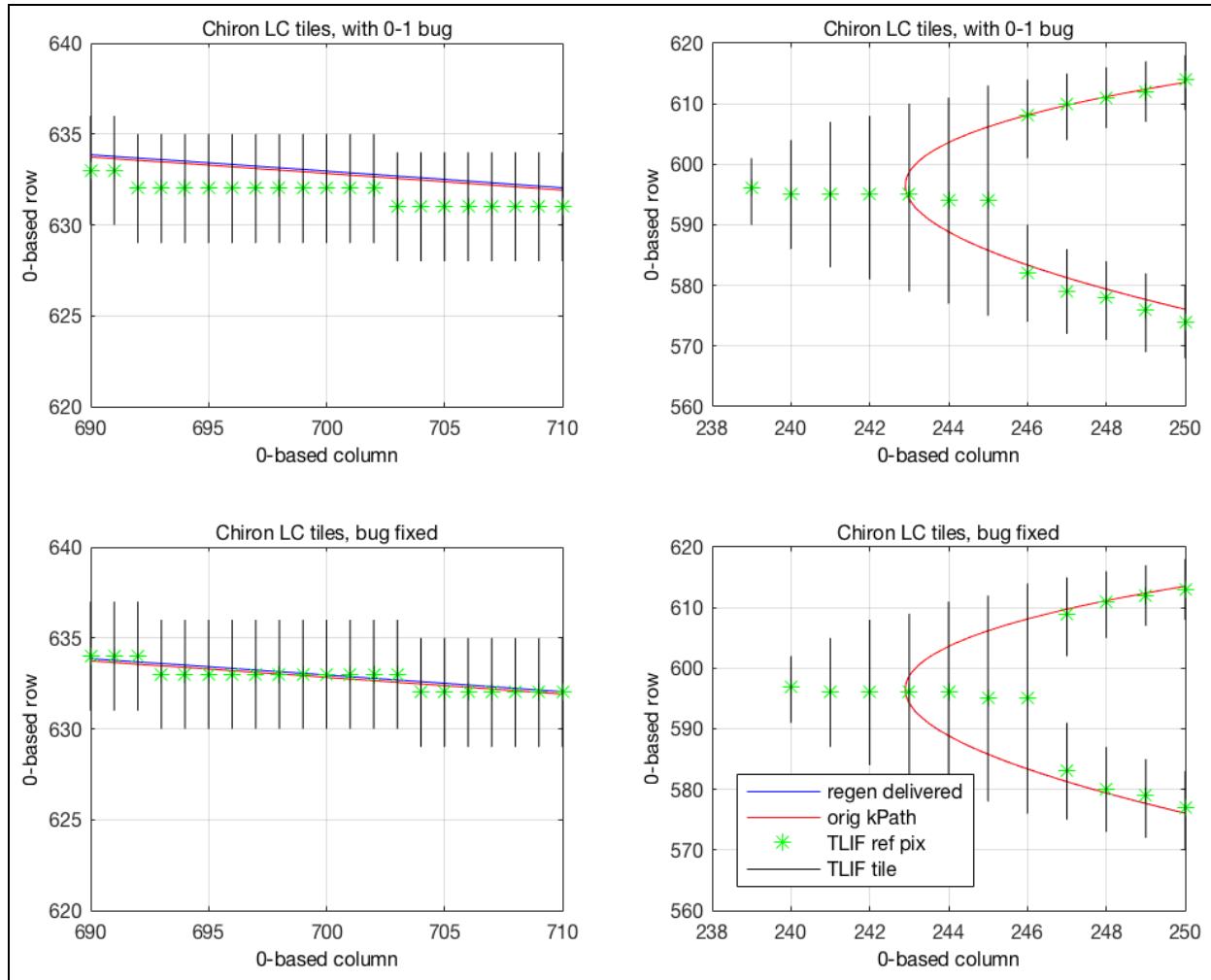


Figure 8: An example of the zero- versus one-based indexing error in SSO tiles using the target Chiron in C12. Upper panels: plots of the requested pixel tiles, based on the target list input file (TLIF), for part of Chiron’s straight path (left) and at its ansa (right). Lower panels: same as the upper panels but using the corrected algorithm. The regenerated and original target paths are the blue and red lines, respectively, and show that the target path pixel coordinates were correctly calculated to better than 0.1 pixels.

2.2.5. Bright Stars

TAD will compute optimal photometric apertures for bright stars ($K_p < 6$) that are exceedingly large as charge bleeds across the array, since the TAD algorithm expects that good photometry cannot be done unless all the bleeding charge is captured in the OA. Furthermore, the statistical mask design process aimed for efficient results only for stars fainter than $K_p > 9$, so the large bright star apertures were not efficiently fit, compounding the pixel consumption. A 6th magnitude star, for example, typically had an aperture containing 4000 pixels, of which ~25% are excess, i.e., not in the OA, but in the target aperture because of the limitation of the finite mask set available. To remedy this problem, many bright stars were given custom apertures that were a fixed disk of 24 to 40 pixels diameter, centered on the star. Photometry of these bright stars has been successfully computed by modeling the wings of the point spread function (Pope et al 2016; Pope et al 2019). The resulting data product is available at the MAST as a High Level Science Product (named HALO; see §4.2.1). HALO will usually be more appropriate for an analysis than the pipeline photometry for these custom targets.

2.2.6. Galaxies

For extended emission from galaxies less than 40 arcsec in radius, the targets were listed in the EPIC and the stellar target list as if they were stars with an effective point source magnitude, and were given extra halos (but no undershoot columns; see KIH §6.6) to capture the additional emission. For galaxies of > 40 arcsec diameter, a custom disk of fixed radius was defined since > 10 halos (masks ~ 25 pixels maximum linear dimension) may have led to inefficient mask selection in TAD.

2.2.7. Extended Regions of the Sky

Regions of high stellar density, such as star clusters, stellar associations, and the galactic bulge were observed by tiling together smaller masks. If the area of the sky exceeded the typical aperture dimensions in the K_p range for which TAD generated efficient mask sets ($K_p > 9$, corresponding to masks of ~ 25 pixels maximum linear dimension), the region was covered with smaller masks, referred to “superapertures” or “superstamps”. Two examples are the five superapertures for the gravitational lensing observations in C9, which were assembled from 1748 custom aperture masks, and the star cluster M67 in C5, C16, and C18. Cody et al. 2018b provides a catalog of all 29 open clusters and associations covered by superapertures throughout K2, and Cody et al. 2018a provides an High Level Science Product (see §4.2.1) for M8, M35, M67, and Ruprecht 147, where the TPFs for each of those extended sky regions were stitched together into spatially contiguous FITS images (one per cadence) for easier scientific analysis.

2.2.8. Reduced Number of Nontarget Science Pixels

Because of the lower pixel budget in K2 compared to Kepler, the Artifact Removal Pixels (ARPs; Van Cleve 2008) were made spatially sparser starting in C2; C0 and C1 had a full set. There were 3355 ARP pixels per channel C0 and C1 (same as Kepler), while only 1174 ARP pixels per channel for C2–C19. The number of background pixels was also reduced after C0. No reverse-clock (RC) pixels (KIH §5.1) were collected in K2.

2.3. Data Processing and Pipeline Updates

Due to the significant changes in target types, pixel allocation, and spacecraft behaviour, the Kepler pipeline required modification to work with K2 data. Users should refer to the KDPH for a comprehensive description of the Kepler pipeline. For K2, the main differences were:

- The K2 pipeline did not perform a planet search nor planet data validation.
- Two thruster firing flags were added to the QUALITY column (see MKAM Table 2-3).
- PDC used 12 basis vectors instead of 8 to better correct the systematics due to the roll motion during the K2 mission.

In the pipeline, a data-driven OA is calculated and used for all cadences to generate lightcurves (see §2.2.1). While this approach worked well in a pipeline application that was designed to be agnostic of scientific content, individual users may find that apertures which move or change shape from cadence to cadence might be best for their particular science. Similarly, neither the Kepler nor K2 pipeline included functionality to generate high precision photometry from custom apertures (see descriptions in §2.2.4 - 2.2.7). While light curves are produced for these apertures, they are generally not the best representation of the photometric behavior of the target of interest. For example, the pipeline has no capability to perform photometry of moving objects (e.g., SSOs, §2.2.4). Similarly, when multiple stars fall within a custom aperture (for example, within a superstamp), the returned light curve is for the entire aperture. In this case, the returned photometry is a blend of the flux from multiple stars. The pipeline-produced target pixel files for custom apertures however do contain appropriately calibrated pixels. In some cases High Level Science Products (see §4.2.1) have been generated by the community to facilitate the study of targets observed via custom apertures.

As successive campaigns were processed, some bugs and nonoptimal parameter values were found and corrected/updated as described in each data release note. With more K2 data in-hand, better ways to process the K2 data were also investigated and implemented, and as a result the pipeline was updated and had settings modified.

From 2018–2020, the K2 mission performed a uniform global reprocessing of the C0–C8 and C10–C14 K2 data with an updated, final version of the Kepler/K2 pipeline; C15–C19 were processed with the same pipeline version. C9 was not reprocessed due to the high stellar density in the C9 field and unique nature of the microlensing experiment conducted during this campaign. This reprocessing was designed to enhance the scientific return of the K2 mission by providing users with a high quality, uniformly processed and documented K2 data set. Each reprocessed campaign was delivered to MAST as soon as it was available. The most recent processing is the default data served to users when obtaining data from MAST (see §4.1). While overall the data improved as a result of reprocessing, in a few limited instances there was a degradation of data quality. In those cases, users may want to use the older version of their data for science analysis (see §2.3.3). The older data remains available to users at MAST — at the time of this writing they are provided via tar archive files in the following subdirectories (<http://dx.doi.org/10.17909/t9-v1ae-7k16> and <http://dx.doi.org/10.17909/t9-xp0s-kn50>).

Each data processing was assigned a data release number, starting with 1 for the initial release of Campaign 0, and ending with 40 for the reprocessing of Campaign 14. With the exception of data release 10, each data release corresponded to a specific individual campaign. Campaigns that had their data processed more than once (C0–C8 & C10–C14) have separate data release numbers for their original processing and their reprocessing(s). Table 5 lists the release numbers associated with each campaign, and Table 6 conversely lists the campaigns associated with each data release number. Note that data release numbers 13 and 16 were assigned to data that were never delivered to MAST. Data releases 21–33 & 35–40 comprise the set of uniformly processed data (shown as bold in Table 5; also referred to as the “final” data release for each campaign). Data release 34 was a release of older C2 data to address a processing bug (see §2.3.3.1). These release numbers are given in the header of each delivered FITS file, and each data release number has an associated data release note document available at MAST (<http://dx.doi.org/10.17909/t9-t116-2c60>), as described in §1.1.

Table 5: K2 Data Release Numbers associated with each K2 Campaign.

Campaign	K2 Data Release Numbers	Campaign	K2 Data Release Numbers
C0	DR01, DR02, DR16 [†] , DR28	C10	DR15, DR37
C1	DR03, DR14, DR32	C11	DR17, DR30
C2	DR04, DR13 [†] , DR21 , DR34	C12	DR18, DR39
C3	DR05, DR10, DR26	C13	DR19, DR24
C4	DR06, DR10, DR33	C14	DR20, DR40
C5	DR07, DR10, DR31	C15	DR22
C6	DR08, DR35	C16	DR23
C7	DR09, DR36	C17	DR25
C8	DR11, DR38	C18	DR27
C9	DR12	C19	DR29

[†]Data Release Number was assigned to a processing of data that was never delivered.

Table 6: K2 Campaigns associated with each Data Release Number.

Data Release	Campaign	Data Release	Campaign	Data Release	Campaign	Data Release	Campaign
1	C0	11	C8	21	C2	31	C5
2	C0	12	C9	22	C15	32	C1
3	C1	13 [†]	C2	23	C16	33	C4
4	C2	14	C1	24	C13	34	C2
5	C3	15	C10	25	C17	35	C6
6	C4	16 [†]	C0	26	C3	36	C7
7	C5	17	C11	27	C18	37	C10
8	C6	18	C12	28	C0	38	C8
9	C7	19	C13	29	C19	39	C12
10	C3,C4,C5	20	C14	30	C11	40	C14

[†]Data Release Number was assigned to a processing of data that was never delivered.

The following subsections describe the list of pipeline changes that went into effect for the global uniform reprocessing effort, and are grouped into two categories: Major and Minor. The Major changes affect the data at a significant level and/or are applicable to the vast majority of campaigns. The minor changes affect the data at a much less significant level and/or are applicable to only a small number of campaigns. Two figures are given below that show which campaigns were affected by each change.

2.3.1. Major Changes

Five major changes were identified and implemented during the reprocessing. These changes include improved background correction, better cosmic ray identification, more effective assessment of spacecraft pointing, and production of short-cadence light curves. Figure 9 shows which campaigns had these major changes in-place for the original processing, and which only had it in place for the reprocessing.

2.3.1.1. Improved Background Correction (Dynablack)

The Kepler pipeline had a feature called Dynamic Black Correction, or “Dynablack” (see KDPH §4). As described in the KDPH, “Dynablack analyzes the black measurements made on the nominal long cadence data and the FFIs to establish thermal corrections to the black correction coefficients used in the calibration module. Dynablack also flags instances of rolling band anomalies, which can inject transit-like features into the science data, causing spurious detections in the transiting planet search.” Compared to *Kepler*, K2 had faster and higher amplitude temperature changes, and thus rolling bands are expected to occur more frequently and with greater amplitude (see Figure 5 of DRN 38 for an example from Campaign 8). As shown in Figure 9 under “Improved Background Correction”, Dynablack was originally not implemented for campaigns prior to C15, but was implemented for the global reprocessing effort such that now C0–C8 and C10–C19 (data releases 21–33 & 35–40) have been processed with it.

	C0	C1	C2	C3	C4	C5	C6	C7	C8	C9	C10	C11	C12	C13	C14	C15	C16	C17	C18	C19
Improved Background Correction	✓	✓	✓	✓	✓	✓	✓	✓	✓	-	✓	✓	✓	✓	✓	✓	✓	✓	✓	✓
Better Identification of Bad Spacecraft Pointing	✓	✓	✓	✓	✓	✓	✓	✓	✓	-	✓	✓	✓	✓	✓	✓	✓	✓	✓	✓
Better Identification of Good Spacecraft Pointing	✓	✓	✓	✓	✓	✓	✓	✓	✓	-	✓	✓	✓	✓	✓	✓	✓	✓	✓	✓
Improved Cosmic Ray Correction	✓	✓	✓	✓	✓	✓	✓	✓	✓	-	✓	✓	✓	✓	✓	✓	✓	✓	✓	✓
Short Cadence Lightcurves Produced	✓	✓	✓	✓	✓	✓	✓	✓	✓	-	✓	✓	✓	✓	✓	✓	✓	✓	✓	✓

Figure 9: The status of major processing features for each K2 campaign. Check marks indicate that the feature is available in the final data release for that campaign. Blue check marks are features/improvements added as a result of the global uniform reprocessing effort.

Dynaback uses the full frame images and collateral pixels to provide two main benefits compared to traditional pixel calibration:

- Improves the correction of science pixels affected by thermally dependent crosstalk from the fine guidance sensors.
- Identify rolling-band artifacts (see §6.7 of the KIH) with flags in the FITS files.

Users can track rolling-band artifacts using the new RB_LEVEL flags in the FITS target pixel files. See §A.1.1 of the Kepler Data Release 25 Notes and §2.3.2 of the MKAM for information on how to interpret and utilize the RB_LEVEL flags. Users should note that the RB_LEVEL flags at durations greater than 6 cadences (3 hours) provide the best indication of the presence of rolling band artifacts. In contrast, the two shortest durations (3 cadences / 1.5 hours and 6 cadences / 3 hours), are overly sensitive to instrument noise and do not offer a reliable indicator of the presence of rolling band pattern noise (KIH §6.7.1). Since the binary “Rolling Band Detected” QUALITY and SAP_QUALITY flags (bits 18 and 19; see MKAM Table 2-3) in target pixel files and light curve files are based on a rolling band detection at *any* of the 5 test durations specified by the FITS header keywords RBT DUR_i (where *i* ranges from 1 to 5), *these two flags do not provide a reliable indicator of the presence of rolling band pattern noise*. Users should note that the correct units for RBT DUR_i is the number of long cadences. The units are incorrect in the Kepler DR25 data release, the latest K2 C2, C13, C15, and C16 FITS files (K2 data releases 21–24), and in MKAM sections 2.3.2 and 2.3.7.

2.3.1.2. Better Identification of Good Spacecraft Pointing

As mentioned in §2.1.4, software on-board the spacecraft determines when the spacecraft is not in fine point. During the original processing of C0–C14 (data releases 1–20) the pipeline would use this information to flag cadences as “Spacecraft is not in fine point” (QUALITY flag bit #16, decimal=32768). The corresponding data was gapped in both SAP flux and PDCSAP flux light curves. When the on-board software was changed to increase the sensitivity of this flag, evaluation revealed it was set on cadences that actually contained good data, where the spacecraft pointing was acceptable for science observations.

The “Spacecraft is not in fine point” flag was used to gap data in the original processing of C0–C14 (see KDPH §5.2.5). For C15–C18, as well as the reprocessing of C0–C8 and C10–C14 (data releases 21–29, 30–33 & 35–40), this flag was ignored in the pipeline. However, this flag was used to gap data for C19 due to a unique case of erratic pointing as a result of fuel exhaustion (see data release note 29 for details). See the next section, “Better Identification of Bad Spacecraft Pointing”, for how cadences with poor pointing were appropriately handled in the pipeline during final processing.

2.3.1.3. Better Identification of Bad Spacecraft Pointing

For the original processing of C0–C13 (data releases 1–19) the "Spacecraft is in coarse point" flag (QUALITY flag bit #3, decimal=4; see MKAM Table 2-3) was not used by the pipeline. However, prompted by the change made to the "Spacecraft is not in fine point" flag described in §2.1.4 and §2.3.1.2, for the original processing of C14–C19 and the reprocessing of C0–C8 and C10–C14 (data releases 20–33 & 35–40), the pipeline was changed to use the "Spacecraft is in coarse point" flag to identify cadences with significant pointing error (see KDPH §5.2.5). For these data releases, this flag was set for each cadence based on the measured pointing error obtained from high-frequency 4-second telemetry. The flag was set if either of the following two conditions were met. This criteria was applied to both short and long cadence data:

- If the 4s telemetry pointing error exceeded 2.5 pixels during a cadence, the cadence was flagged.
- If the 4s telemetry pointing error exceeded 1.5 pixels during a cadence, for each of 4 or more contiguous cadences, then all 4 (or more) cadences were flagged.

The pipeline treats these "coarse-point" cadences by gapping them in the PDCSAP light curves for the flagged cadences. (Note that SAP light curves were not gapped based on this flag.) The mission found that implementing this flag significantly improved the measured precision of the PDCSAP light curves, both as a result of eliminating flux outliers due to poor pointing and due to improved performance by the PDC algorithm. In the absence of outliers, PDC was able to perform improved detrending of broad systematics. With the completion of the global reprocessing of K2 observations, the mission recommends that users look to QUALITY and SAP_QUALITY flag bit #3 as an indicator of poor spacecraft pointing during the entire K2 mission.

2.3.1.4. Improved Cosmic-Ray Correction

The cosmic ray (CR) detection and correction algorithm (see KDPH §6.3.1) was developed using the observed characteristics of Kepler mission data. The design assumed wide-sense stationary data, for which the mean is constant and autocorrelation depends only on the time separation between points. K2 mission data is not wide-sense stationary, since autocorrelation is time dependent — the correlation between data points separated by a fixed time interval changes with absolute time due to the roll cycle of the *Kepler* spacecraft. Roughly speaking, motion-induced changes in flux on a given pixel can be mistaken for signal discontinuities produced by cosmic rays. This was recognized early in the K2 mission, and CR detection and correction were turned off for target pixels for all of K2. However, CR detection was enabled for the collateral data, which generated many false positive detections in the smear and virtual smear when bright targets shifted between adjacent columns due to spacecraft motion. The motion of bright targets generated outliers in the time series of the smear data. Spurious vertical bright streaks were subsequently created when the false positive detections were removed from the collateral data and then the collateral data was subtracted from the science data. Rather than turn off CR detection for collateral data (which would lead to a comparable error from uncorrected CRs) it was found that an increase in the CR threshold from 4 to 7 standard deviations (4σ to 7σ) substantially reduced the number of false positives in the smear and virtual smear, while continuing to do an adequate job of detecting real CRs. This higher threshold was first used in C11 and subsequent campaigns and all of the reprocessed campaigns (data releases 17–40).

CR detection and correction was also used on background pixels (pixels not in the target aperture) throughout the K2 mission. These background pixels were designed not to contain significant stellar flux, and hence are relatively insensitive to image motion induced flux discontinuities.

2.3.1.5. Short Cadence Light Curve Production

Calibrated short-cadence target pixel files were delivered for data releases 1–20 (along with long-cadence target pixel files), and long-cadence lightcurves were delivered for data releases 5–20. However, short-cadence light curves were not delivered for data releases 1–20. Starting with data release 21, short-cadence light curves were produced and delivered in addition to the target pixel files.

The Kepler pipeline corrected short-cadence SAP light curves by interpolating the long-cadence cotrending basis vectors (CBVs) that are produced by long-cadence PDC (see KDPH §8.5.7). This method was not designed to accommodate significant motion and the resulting systematics that arise in K2 data, and as a result often does a poor job of detrending K2 short-cadence data. For this reason, beyond an initial inspection based on C2, the mission initially did not attempt to produce short-cadence K2 light curves as part of its processing for C0–C14 (data releases 1–20).

As part of the global reprocessing effort, the K2 mission revisited the prospect of producing short-cadence light curves, starting with data release 21. In consultation with K2 users, the mission decided that despite the often poor detrending, there was value in having short-cadence light curves available for initial inspection, especially given that currently short-cadence light curves are not produced for most short cadence targets as part of the community-delivered high-level science products (see §4.2.1). The hope was that these pipeline short-cadence light curves may be used for initial inspection of the short-cadence data, which might prompt users to perform their own short-cadence detrending, or better adapt the existing long-cadence Cotrending Basis Vector (CBV) files for use in detrending the short-cadence data.

Short-cadence light curves have been delivered for all K2 campaigns (data releases 21–33 & 35–40), except for C9, which did not have any light curves (short- or long-cadence) produced due to its extreme stellar density (see Figure 2). However, users are strongly cautioned that no work was done to adapt the Kepler pipeline's detrending module (PDC), developed for Kepler data, to work well on short-cadence K2 data. Thruster firings are especially poorly corrected for many short-cadence targets, and other systematic features may not be corrected well. See the middle panel of Figure 16 for an example of remaining systematics in short-cadence data around thruster firings. However, some short-cadence targets do have adequate detrending in their short-cadence light curves — especially if the target exhibits astrophysical flux variations and was observed with a sufficiently large aperture to adequately capture the peak flux brightness. For example, Figure 10 shows the C15 long- and short-cadence SAP and PDCSAP light curves for the cataclysmic variable star HP Lib (a AM CVn type binary); its ~18 minute periodic variations are readily apparent in the K2 short-cadence data.

2.3.2. Minor Changes

Six minor changes were identified and implemented during the reprocessing. These changes include improved use of flags to include and exclude data, proper pixel-level calibration in the presence of very bright stars, correction of minor software bugs, and pipeline updates that allowed for the delivery of previously undeliverable targets. Figure 11 shows which campaigns had these minor changes in-place for the original processing, and which only had it in place for the reprocessing.

2.3.2.1. LDE Parity Error Flag Ignored

An 'LDE Parity Error' flag was set on-board the spacecraft for all targets when a bright object on that channel bled into the serial readout register area of the CCD and resulted in an out of bounds value in the analog-to-digital converter. Since this was an extremely rare event during the Kepler mission, the pipeline was set to discard all cadences flagged as 'LDE Parity Error' in both the target pixel and light curve files for all targets (see KDPH §5.2.5). With K2, there were many bright stars and bright, moving planets that occurred in several campaigns. This caused the 'LDE Parity Error' flag to be tripped for multiple cadences in several campaigns. Specifically, 1,237 cadences are flagged in C2 most likely due to the K_p -4 star EPIC 205283834, 128 in C6 most likely due to Spica, 148 in C11 most likely due to Saturn, and between 2–11 cadences in all other campaigns. Inspecting the cadences, the actual data was found not to be defective, and thus these cadences should ideally not be discarded.

As shown in Figure 11, the pipeline was set to discard cadences based on the 'LDE Parity Error' flag for C0, C1, C3, C4, C6, and C8. No ill effects were seen in the other campaigns when the pipeline was set to ignore the flag. In all reprocessed campaigns (data releases 21–33 & 35–40), the pipeline was set to ignore the flag; this resulted in more cadences with good data being available to users.

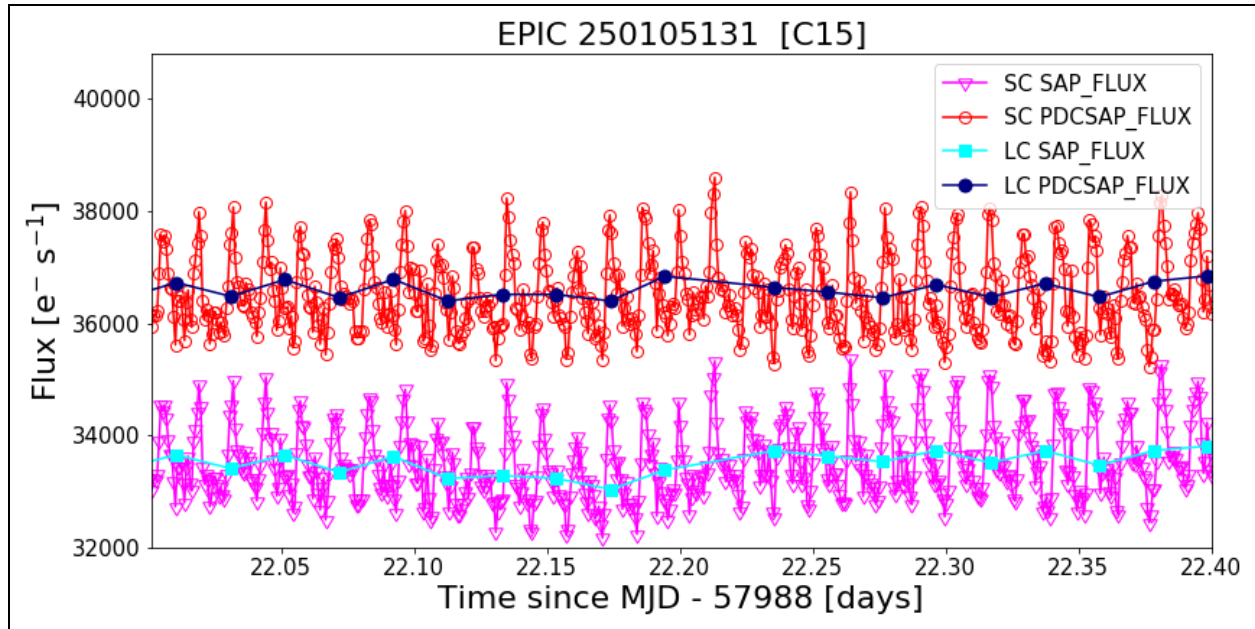


Figure 10: The C15 long- and short-cadence SAP and PDCSAP light curves of the AM CVn type binary HP Lib (EPIC 250105131). The ~18 minute periodic photometric variation is only apparent in the short-cadence data. Note that no offset has been applied to the SAP or PDCSAP light curves — the apparent offset is due to PDC’s long-term trend correction over a campaign and the short (~0.4 day) plot scale.

	C0	C1	C2	C3	C4	C5	C6	C7	C8	C9	C10	C11	C12	C13	C14	C15	C16	C17	C18	C19
LDE Parity Error Flag Ignored	✓	✓	✓	✓	✓	✓	✓	✓	✓	✓	✓	✓	✓	✓	✓	✓	✓	✓	✓	✓
Momentum Dump Flag Used	✓	✓	✓	✓	✓	✓	✓	✓	✓	-	✓	✓	✓	✓	✓	✓	✓	✓	✓	✓
Bright Star Smear Corrected Properly	✓	✓	✓	✓	✓	✓	✓	✓	✓	✓	✓	✓	✓	✓	✓	✓	✓	✓	✓	✓
FFI Interpolation Bug Fixed	✓	✓	✓	✓	✓	✓	✓	✓	✓	✓	✓	✓	✓	✓	✓	✓	✓	✓	✓	✓
Scrambled Uncertainties Bug Fixed	✓	✓	✓	✓	✓	✓	✓	✓	✓	-	✓	✓	✓	✓	✓	✓	✓	✓	✓	✓
All Target Files Delivered	✓	✓	✓	✓	✓	✓	✓	✓	✓	✓	✓	✓	✓	✓	✓	✓	✓	✓	✓	✓

Figure 11: The status of minor processing features for each K2 campaign. Check marks indicate that the feature is available in the final data release for that campaign. Blue check marks are features/improvements added as a result of the global uniform reprocessing effort.

2.3.2.2. Momentum Dump Flag Used

A “momentum dump” flag (QUALITY and SAP_QUALITY flag bit #6, decimal=32 : “Reaction wheel resaturation event”; see MKAM Table 2-3) was set on-board the spacecraft for all targets when the spacecraft initiated a momentum dump (a.k.a. a ‘re-sat’). This happened about every 2 days as part of normal K2 operations to maintain spacecraft pointing with two reaction wheels. During this time, the

spacecraft would move up to half a degree within a cadence, which will significantly affect the ability to measure accurate photometry during an affected cadence.

The Kepler pipeline was nominally set to discard cadences flagged as 'Momentum Dump' in both the target pixel and light curve files (see KDPH §5.2.5). As shown in Figure 11, the pipeline utilized the 'Momentum Dump' flag for C0–C5 (data releases 1–7) and C11–C19 (data releases 17–29) in the original reprocessing. For the C6–C10 original processing (data releases 8–15), the mission experimented with setting the pipeline to ignore the flag, as there was a possibility that some of these flagged cadences did not have significant motion and might produce accurate photometry. However, upon examination based on the original C6–C10 data, the mission found that indeed these flagged cadences should be discarded and accurate photometry was not able to be recovered for them. All campaigns (except for C9) were reprocessed with the pipeline set to discard cadences flagged as 'Momentum Dump' (QUALITY and SAP_QUALITY bit #6, decimal value = 32) in both the target pixel and light curve files (data releases 21–33 & 35–40). This resulted in ~40 fewer cadences per campaign for C6–C10, but improved PDC light curves as detrending power was not wasted correcting outliers resulting from momentum dumps.

2.3.2.3. Campaign 13 Bright Star Smear Corrected Properly

In C13, the first magnitude star Aldebaran on channel 73 bled heavily into the serial register of the CCD, corrupting the first three rows of the masked smear region (see KDPH §5.3.7). While these rows were not used for the smear correction, at times during C13, the saturation spill covered more rows in the masked smear, extending up to row 15 on channel 74. Pipeline calibration fits a linear model to trailing black rows 7-18 to estimate the black (bias) level for the masked smear region. In this instance, the trailing black estimate for the masked smear signal was corrupted, resulting in a corrupted smear signal that was then applied to all pixels on the channel. As a result, all targets on channel 74 were affected for these cadences, resulting in light curves that showed significant 'chatter' in baseline flux level for affected cadences. The black and smear corruption effects were most prominent in the first 80 cadences of the campaign and again in the period between cadence 1800–3200. The net effect was to render the data for targets on channel 74 in C13 (data release 19) nearly unusable for science study (without significant work by users to recalibrate the pixel data).

As shown in Figure 11, under "Bright Star Smear Corrected Properly", this effect was unique to C13. When C13 was reprocessed (data release 24), the black level model coefficients for channel 74 were manually set to fixed values for all cadences, thus producing nominal data for channel 74 targets. The value of these new coefficients were determined by the mission instrument scientist based on data from campaigns 4 and 8, which exhibited similar behavior in this channel compared to campaign 13.

2.3.2.4. Full Frame Image (FFI) Interpolation Bug Fixed

Full Frame Images are used to supplement the pixel-level undershoot correction (see §5.3.6 of the KDPH). When a K2 campaign had more than one Full Frame Image, the Kepler pipeline interpolated data between those FFIs, and extrapolated before and after each, to account for variations over time when calibrating the pixel level data. A bug was discovered where FFIs from later campaigns were used to interpolate for calibration of the current campaign. This bug affected the pixel-level data, and thus light curves as well. Since there are usually two FFIs per campaign, taken ~1/3 and ~2/3 the way through a given campaign, for the last ~1/3 of a campaign the interpolation was between the last FFI of the current campaign and the first FFI of the next campaign (which had, by definition, a different field-of-view). Thus, the latest cadences of the campaign are affected the most by this bug. The exact impact of the effect is not known, but is thought to be small given that the FFI data are only used to supplement the undershoot correction (see KIH §6.6 and KDPH §5.3.6) in calibration and the interpolation will weight the FFI values towards the correct campaign.

Because campaigns were predominantly processed in the order they were observed, the only publicly available data release affected was DR14 of C1, as this processing occurred after FFIs for later campaigns were available. This bug was fixed prior to reprocessing.

2.3.2.5. *Scrambled Uncertainties Bug Fixed*

A bug in the Kepler pipeline was discovered that caused the uncertainties on the smear calibration data for each column to be randomly scrambled. While each column's smear value was correct, it had a random uncertainty from another column, which can vary by ~20% column-to-column. When these uncertainties are propagated into the pixel-level flux value uncertainties (see KDPH §8.5.6), it results in incorrect flux uncertainties on the level of ~0.3%. The biggest impact this has is on the selection of the optimal photometric aperture by PA-COA (see KDPH §7), due to the algorithm's sensitivity to uncertainties. Tests performed by the mission with the bug present versus the bug fixed confirm that while the bug had no significant effect on overall photometric precision, it did cause a significant change in the photometric aperture selected for a small number of targets. As shown in Figure 11, the original processings of C0–C10 (data releases 1–15) were affected by this bug before it was detected and corrected in time for all subsequent data releases, including the reprocessing of C0–C8 and C10.

2.3.2.6. *Target Files Delivered*

During the original processing for three campaigns (C2, C11, and C14) some targets did not have target pixel and/or light curve data delivered for various reasons. For data releases 1–4, no light curves were delivered as the Kepler pipeline had not been fully adapted to work for K2 at the time, and until the code was finalized, it was deemed best to just produce target pixel files. For C2, C11a, C11b, and C14 (data releases 4, 17, & 20), there were 2–3 targets each that had an error when computing their centroids such that no World Coordinate Solution (WCS) information was available and a FITS file could not be created for those targets, and thus no target pixel files nor light curves were delivered. For C11b (data release 17), there were 191 targets that did not have delivered target pixel files or light curves due to a bug in how the pipeline FITS file creator was configured to run. When these campaigns were reprocessed (data releases 21, 30, & 40), these issues were fixed/addressed and the missing targets were delivered for those campaigns. See §2.3.3 below for other known issues remaining with the K2 data releases.

2.3.3. **Significant Remaining Processing Issues**

Users should refer to the data release note for each campaign for information and analysis of any features of a campaign that may pose a data analysis challenge (e.g., Mars crossing the field in C5, bright stars that saturate the detector, regions of high stellar density, etc.). Also, major processing issues (cases where science analysis is significantly impacted), and minor processing issues (cases where a limited number of targets were impacted by pipeline bugs or non-optimal settings at a level unlikely to significantly affect science analysis), are both documented in the DRN. For visibility, this section highlights the major processing issues that remain in the final data release for one or more campaigns.

2.3.3.1. *Pixel Mapping Reference File (PMRF) Bug*

A bug in the implementation of the Pixel Mapping Reference File (PMRF) significantly affects the calibrated data in some of the short-cadence target pixel files (and resulting short-cadence light curves) for the reprocessed C2, C3, and C5 data (Data Releases 21, 26, and 31). Users should read Data Release Note 34 (<http://dx.doi.org/10.17909/t9-t116-2c60>) for details, lists of affected targets, and diagnostics. Users whose target is affected are encouraged to use data from an unaffected data release, specifically data release 34 for C2 and data release 10 for C3 and C5.

2.3.3.2. *Proper Motion Bug*

Wolf 359 (EPIC 201885041) is a high proper-motion (~4.7"/yr) target in C14. Due to an error in pipeline configuration for the data release 40 processing, the proper motion was not taken into account. As a result, there was no optimal photometric aperture generated for the target, and thus no long- or short-cadence light curve files were produced. (The target pixel files, aside from not having any pixels identified as belonging to an OA, were not affected.) Users are encouraged to create their own light curves for this object from target pixel files.

In C15 (see data release note 22) it was noticed that the high proper-motion target Ross 802 (EPIC 250111823) had a PDCSAP light curve flux that was orders of magnitude greater than the SAP light curve flux. Similar to Wolf 359 in C14, the issue was traced to improper handling of the target's proper motion. It is possible that multiple campaigns are affected by this issue. Users are encouraged to check for potentially mis-scaled PDCSAP FLUX for any target with accumulated proper motion since J2000 of ~ 1.5 pixels (~ 6 arcseconds) or greater.

2.3.3.3. Sub-Optimal Smear Correction

In the original C8 processing (data release 11), it was noted that there were episodic smear correction errors on channel 42 (mod.out 13.2) — the channel containing the Uranus superstamp. Preliminary investigation indicated that the streaking was due to false cosmic ray detections in the smear collateral data, and so the cosmic ray detection threshold was adjusted (see §2.3.1.4) for the final processing (data release 38). However, paradoxically the smear errors were worse in data release 38 than data release 11, likely due to other issues as a result of Uranus — users are thus encouraged to consider using data release 11 when working with the Uranus superstamp or any other targets on channel 42 in C8.

For data release 40, channel 74 in campaign 14 had an improper smear correction that results in an additive effect at the pixel-level, with two step-wise discontinuities. The cause of this improper correction appears to be unexpected behavior from Dynaback (see §2.3.1.1) due to outlier calibration data unique to this channel. Users are cautioned to be aware of this effect when interpreting any signals for their science, and may want to use data release 20 for analyzing targets on channel 74 in campaign 14.

2.4. File Formats

K2 file names, in general, have changed from `kp1r*.fits` to `ktwo*.fits`, and minor changes to the FITS headers were made as appropriate. The `MISSION` FITS keyword value was changed to become 'K2'. The `QUARTER` FITS keyword was replaced with the `CAMPAIGN` FITS keyword. The `SEASON` FITS keyword was no longer used. The K2 archive at MAST has the same types of files and file formats as Kepler (MKAM §2.3), with these two exceptions: 1) there are no longer any RC (reverse-clock) data files, and 2) there is a new type of target pixel file (TPF), called "Type-1".

Standard K2 target pixel files, called "Type-2" TPFs, were produced as part of all data releases that produced light curves. When it was not possible to run the portions of the pipeline which generated lightcurves, Type-1 TPFs were produced. Type-1 TPFs differ from Type-2 TPFs in three ways: 1) Type-1 WCS are less precise, 2) thruster firing flags (see MKAM Table 2-3) are not populated in FITS QUALITY flags, and 3) no background subtraction is performed.

Regarding item 1, Type-2 TPFs have WCS coordinates based on the reconstructed pointing, aberration, and local optical distortion determined from the measured PRF centroid motion of a number of bright unsaturated stars across each channel. This motion polynomial model (KDPH; Van Cleve 2010) tracks the roll drift and any impulsive pointing offsets, resulting in reconstructed position errors at or below 0.1 pixel for each cadence. The FITS header reports only the WCS derived from the motion polynomials for the middle cadence of the campaign, so users of K2 data will have to use the `POS_CORR` centroid offsets from the corresponding light curve file to offset the WCS for individual cadence K2 target pixel images in the Type-2 pixel files. Unless discussed elsewhere in this document, all calibrations and QUALITY flags are set in Type-2 TPFs as they were for Kepler.

In contrast, Type-1 TPFs have a WCS based on a focal plane model (see MKAM §2.3.5.14-16) and commanded pointing, rather than using the science data to empirically reconstruct a pointing history of the K2 observations. The WCS coordinates in Type-1 TPFs can be off by 1–2 pixels due to the unmodeled roll motion and discrete pointing offsets (§3.2). See §3.5 for an independent assessment of WCS fidelity.

Regarding item 2, as mentioned in §2.3, the Kepler pipeline was modified for K2 to add flags to indicate when thrusters were fired during an observation. However, this code is only called when producing Type-2 TPFs, and thus Type-1 TPFs do not have these flags populated. Regarding item 3, as described in §6.3.2 of the KDPH, background estimation and subtraction in the Kepler/K2 pipeline requires running the PA module. Since PA is not run when producing Type-1 TPFs, background estimation and subtraction is not performed, and thus the reported flux for Type-1 TPFs will be a sum of that from the background and astrophysical sources.

In the early days of the K2 mission, calibrated target pixels were released to the community before the software was updated to produce light curves under K2 observing conditions. This was done in order to provide K2 data to users as early as possible. These results were released in Type-1 TPFs. As a result of global reprocessing, all campaigns except C9 and C10a now have the standard Type-2 TPFs. Type-1 TPFs were produced for C9 because most pixels were in superapertures (see §2.2.7) and there were not enough stars with individual apertures to calculate the required motion polynomials. In C10a, the pointing error at the start of the campaign was large enough to invalidate the assigned photometric apertures, which prohibited lightcurve production. Separate long-cadence and short-cadence thruster firing tables for C9 and C10a are included in their data release notes. Determining accurate WCS coordinates and final background subtraction for these campaigns must be addressed by users.

3. Evaluation of Performance

This section provides an evaluation of various aspects of spacecraft performance and data quality. §3.1 and §3.2 cover the performance of the pixel response function and spacecraft pointing under K2 operations; pointing was considerably different from Kepler. These two factors have the biggest influence on the resulting photometric precision, described in §3.3. §3.4 discusses the performance of data compression and its per-campaign variation. §3.5 briefly discusses the fidelity of the WCS information available in K2 data files. §3.6 discusses the photometric performance of moving targets — a unique type of observation performed by K2. Finally, §3.7 provides a thorough analysis of the spurious frequencies in K2 data, which considerably differ from Kepler due to K2's periodic thruster firings.

3.1. Pixel Response Function

The Point-Spread Function (PSF) of the Kepler photometer varies considerably across the focal plane, due primarily to the Schmidt-telescope optics, which provide a large FOV approximately 16° in diameter. The *Kepler* Pixel Response Function (PRF) is the total response of the instrument to incident light which represents the observed appearance of point sources. The PRF is a combination of the optical design, focus setting, mechanical and electronic properties of the CCD detector, and the temporal sequence of spacecraft pointing stability during an observation. The PRF depends on location within the focal plane (as defined by a source's CCD channel, row, and column location), as well as the *intrapixel* location of the source centroid (peak incident light). A detailed summary of the characteristics and modeling of the PRF is provided by Bryson et al. (2010). Figure 12 shows two example Kepler mission PRFs.

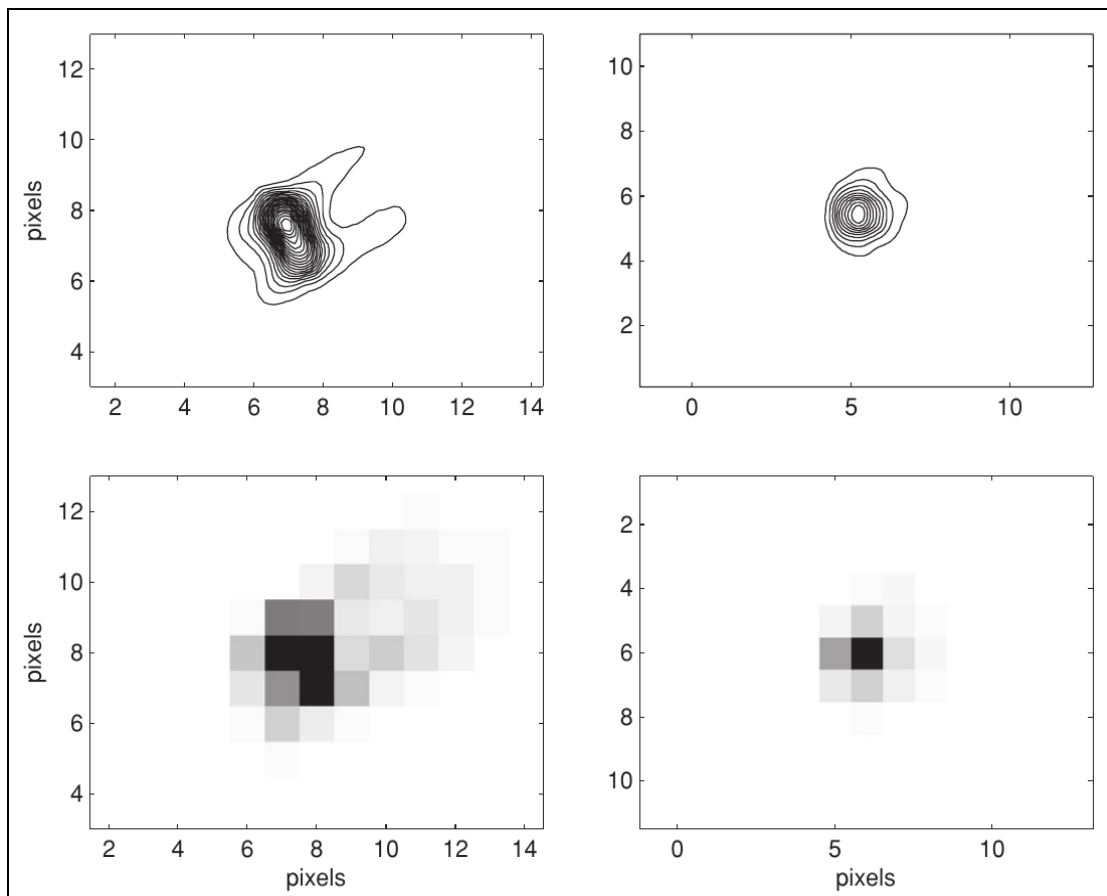


Figure 12: Two example Pixel Response Functions from the Kepler mission (Bryson et al. 2010). The *left* PRF is near the edge of the focal plane and the *right* PRF is near the center of the focal plane. Pixelated images are shown *below* and contour versions are shown *above*.

Figure 13 shows a fit of a Kepler-mission fine-point Point-Spread Function to a K2 image (PRF) of a coarse-point target that was close to the boresight of the *Kepler* spacecraft during engineering tests. Spacecraft jitter during a long-cadence exposure in two-wheel operation is generally only a few percent larger than the three-wheel Kepler mission and is not a major concern for K2 photometric precision.

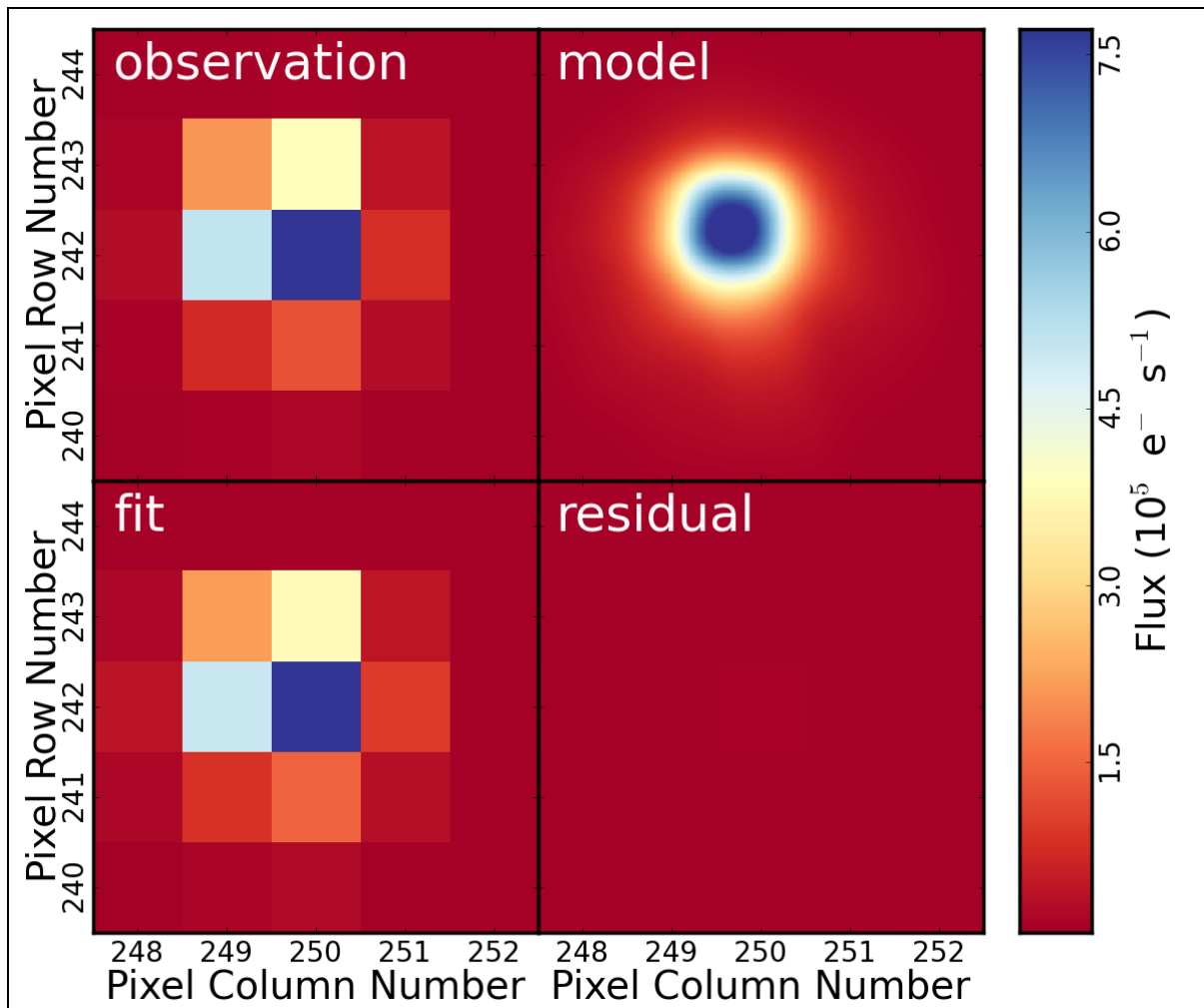


Figure 13: The fit of a Kepler fine-point PSF to a K2 image (PRF) of a coarse-point target close to the spacecraft boresight. From top-left to bottom-right: a 30 minute observation of a 12th magnitude K2 star, the best-fitting Kepler-mission PSF model, the best-fit model binned over detector pixels, and the fit residual.

3.2. Pointing

Pointing stability during the Kepler mission was typically measured in 10's of millipixels, while that during the K2 mission was measured in pixels. Pointing performance was quantified for each campaign using the MAR (maximum attitude residual) metric, which is a per-cadence time-series of the largest distance between the expected and observed location of any target. MAR was calculated by the pipeline Photometer Performance Assessment (PPA) Attitude Determination (PAD) module (see KDPH §2.3.2.1). MAR is presented visually as a time series in the DRNs, while a statistical summary of the time series is shown in Table 7. MAR includes the initial constant pointing error (the offset of the telescope's boresight from the desired field of view center) as well as motion throughout the campaign (the roll angle change due to photon pressure and thruster firings). Roughly speaking, the 10th percentile MAR is the constant part of MAR and the difference between the 10th and 90th percentiles quantifies the variation of MAR.

Table 7: Summary statistics for each campaign of the Maximum Attitude Residual (MAR) in units of science pixels. The data release notes for each campaign discuss reasons for unusually large MAR values (e.g., the 90th percentile MAR is noticeably worse in C7 than other campaigns). There are no MAR statistics for C9 and C10a since light curves were not generated and the PPA-PAD module was therefore not run. Gapped data are excluded from these statistics.

Campaign	10 th p	Median	90 th p	99 th p	Max
0	0.42	0.91	1.42	1.85	4.99
1	0.25	0.61	1.13	1.55	1.92
2	0.22	0.58	1.16	1.64	4.72
3	0.28	0.58	1.10	1.68	2.06
4	0.19	0.49	0.96	1.41	1.99
5	0.38	0.77	1.28	1.61	1.86
6	0.33	0.60	1.15	1.63	2.12
7	0.25	0.92	1.84	2.65	3.37
8	0.27	0.64	1.25	1.74	2.29
10b	0.41	0.70	1.16	1.51	1.69
11a	0.49	0.95	1.48	1.95	2.19
11b	0.39	0.90	1.50	1.84	2.13
12	0.31	0.67	1.17	1.65	3.17
13	0.34	0.66	1.18	1.94	3.26
14	0.17	0.50	0.95	1.32	1.73
15	0.34	0.79	1.53	1.97	2.34
16	0.53	0.86	1.35	1.78	2.24
17	0.10	0.45	1.02	1.61	1.95
18	0.38	0.76	1.28	1.60	4.58
19	0.42	0.69	1.10	1.32	1.42

3.3. Photometric Precision and CDPD for Pipeline Light Curves

The photometric precision achieved during K2 is influenced by several factors, including spacecraft jitter during an exposure, the time scale roll motion inherent to 2-wheel operations, the stellar density and presence of bright targets in the field of view of a campaign, and the stability of the guide stars. Two of these factors have been discussed in previous sections — the impact of spacecraft jitter can be assessed by studying the achieved PRF as discussed in §3.1, and the achieved longer time scale pointing performance was discussed in §3.2.

The fine-point photometric precision achieved by K2 in Campaign 3 in comparison to that achieved by Kepler in Quarter 10 is shown in Figure 14. Giant stars were excluded in order to provide a comparison against photometrically-quiet dwarf stars. In this plot, the K2 data was detrended using the method of Vanderberg & Johnson (2014) rather than the pipeline's PDC module. Note that the data from Campaign 3 was taken after applying an increase in pointing control bandwidth, so data in earlier Campaigns will provide slightly poorer photometric precision.

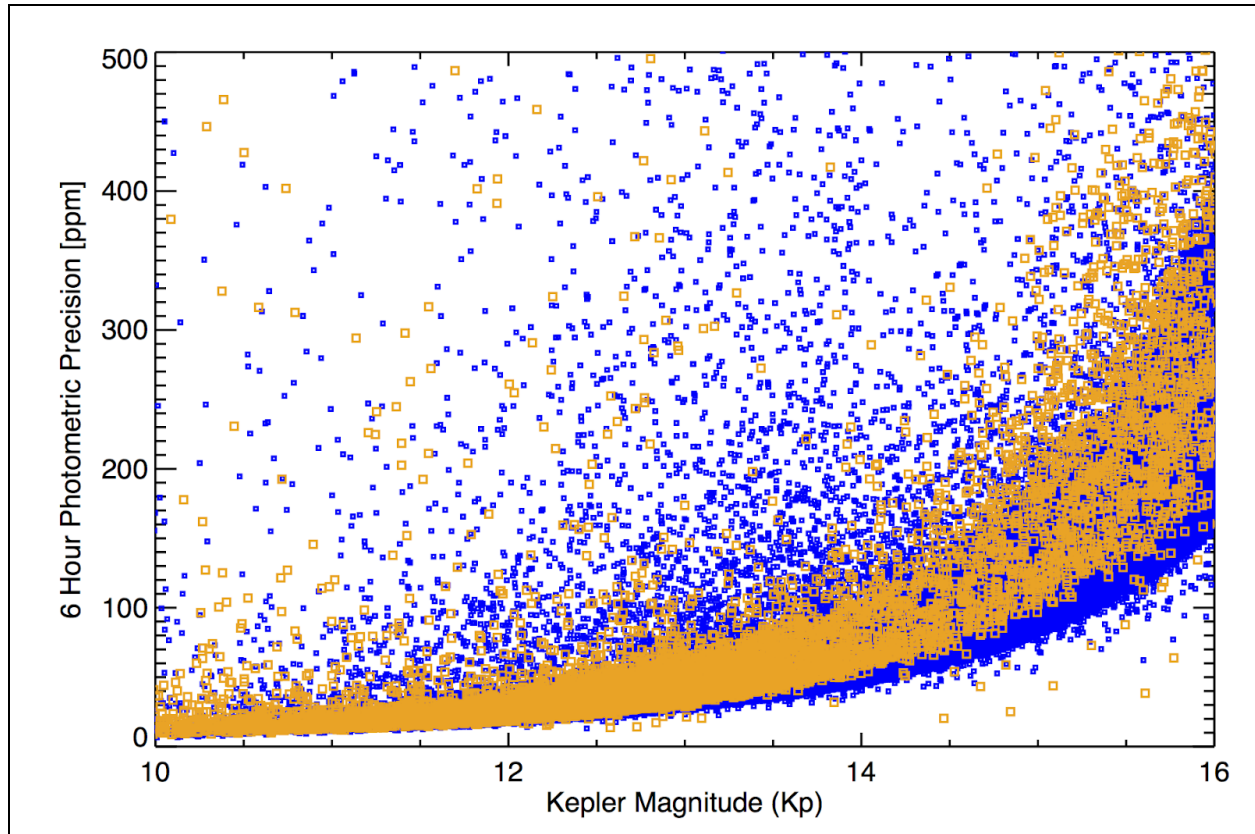


Figure 14: A comparison of the fine-point photometric precision achieved by K2 in Campaign 3 (orange) and that achieved by Kepler in Quater 10 (blue). Figure credit: Andrew Vanderburg.

FGS guide star variability can affect K2 photometry by causing periodic pointing offsets. For example, during C6 false signals as large as 1000 ppm were impressed on light curves by the telescope motion induced by a variable guide star; see the C6 DRN (<http://dx.doi.org/10.17909/t9-t116-2c60>) for more details. Users wishing to investigate this topic further should see §4.1.7.

The Combined Differential Photometric Precision (CDPP) was used throughout the Kepler mission as a metric to assess the ease of detecting a transit signature in a star's lightcurve (Christiansen et al 2012). In addition to the factors discussed above that influence photometric precision, CDPP depends on the duration of the transit, the magnitude of the star, and the star's intrinsic variability. The benchmark CDPP for Kepler assesses the detectability of a ~6-hour transit around a 12th magnitude dwarf ($\log g > 4.0$) star. While CDPP is, by definition, a function of time, the median or rms average over a time series for a given star are useful metrics. These per-star values are summarized further as percentiles over groups of stars; for example, CDPP_{10} is the 10th percentile of CDPP over a group of stars. Users may wish to use simpler noise metrics, such as a Savitsky-Golay filter (Van Cleve et al. 2016) or a running standard deviation, to approximate CDPP.

Summary statistics of achieved 6.0-hour CDPP for 12th magnitude stars versus three important factors that can degrade light curve quality are given in Table 8. The factors shown are the motion component (variable spacecraft roll angle) of MAR (90th–10th percentile), the star count n^* , and the presence of bright ($K_p \leq 6$) planets in the FOV. When possible, the PDC pipeline module (see KDPH §8) is used to calculate the per-star rms average CDPP. However, PDC does not produce a meaningful number in the presence of large data gaps, such as that caused by the failure of module 4 in C10b. Thus, as an alternative, the C10b per-star CDPPs were calculated using medians over time, instead of an rms average. The low CDPP for C19 may be an artifact of the short duration of that campaign, making the PDC results

susceptible to overfitting. Additional details about the photometric precision of individual K2 campaigns are given in the K2 DRNs, which include scatter plots and FOV images of CDPP, plots of 6.0-hour CDPP (ppm) measurements for campaign targets as a function of Kepler magnitude, and a table showing CDPP_{10} and CDPP_{50} over the FOV, sorted by magnitude bin.

Van Cleve et al. (2016) examined pipeline light curves for C3–C6 and found that CDPP_{10} increases linearly with distance from the FOV center, in proportion to roll motion, while the CDPP_{10} at the center of the FOV — where roll motion is least — is 30 ppm, only 25% higher than that for Kepler.

Table 8: 6.0-hour CDPP_{10} and CDPP_{50} for 12th magnitude dwarf stars as a function of campaign based on each campaign’s final data release, along with factors that impact photometric precision. CDPP_x is the x^{th} percentile of the temporal rms average CDPP for all campaigns except C10b — the C10b result is the x^{th} percentile of the temporal median since the mod 4 failure data gap made other metrics unavailable. A discussion of MAR can be found in §3.2. The last column gives the stellar density as EPIC stars per square degree for $11.5 < K_p < 14.5$ mag.

Campaign	CDPP_{10} (ppm)	CDPP_{50} (ppm)	$\text{MAR}_{90} - \text{MAR}_{10}$ (pixels)	Bright Planets	n*
0	50.1	191.7	1.00	Jupiter	1054
1	43.5	95.7	0.88		125
2	85.6	139.0	0.94	Mars	569
3	46.1	98.2	0.82		176
4	48.5	96.9	0.77		226
5	41.4	78.2	0.89		251
6	42.7	78.7	0.82		166
7	52.8	102.7	1.58		1618
8	45.7	91.7	0.98	Uranus	133
9	-	-	-		12690
10b	44.3	113.4	0.74		128
11a	50.5	128.9	0.98		7073
11b	58.5	124.8	1.11	Saturn	7073
12	52.6	115.0	0.86	Mars	144
13	49.1	106.9	0.84		338
14	45.6	116.8	0.78		131
15	47.9	99.2	1.19		368
16	45.4	104.9	0.82	Earth	211
17	42.5	113.4	0.92		148
18	41.2	83.8	0.90		255
19	35.8	64.5	1.76	Neptune	153

3.4. Data Compression

Data compression is an essential feature of both the Kepler and K2 missions since on-board data storage is limited by the size of the SSR. As noted in Van Cleve et al (2016), K2 contains more bits of information than Kepler data because of image motion and the high stellar density in some regions of the sky viewed by K2. More information reduces the efficiency of the on board data compression, reducing the amount of data that could be stored. Since every campaign had a different stellar density, the efficiency of the data compression varied from campaign to campaign. In several cases, the execution of campaigns was modified to prevent overfilling the SSR (e.g., early end to C3 and skipped FFIs in C13 and C15).

As succinctly stated in the §2.3.2.5 of the KDCH, “The data compression scheme involves three steps: 1) requantizing the data so that the quantization noise is approximately a fixed fraction of the intrinsic measurement uncertainty (which is dominated by shot noise for bright pixels), 2) taking the difference between each re-quantized pixel value and a baseline value that was updated once per day, and 3) entropic encoding via a length-limited Huffman table (Jenkins & Dunnuck 2011).” More information increases the number of bits per pixel (denoted as B in subsequent discussion) needed to represent the data without significant compression losses. K2 baselines were collected every 12 hours instead of 24 hours in order to accommodate the higher information content.

The Kepler B value was between 4.6 and 5.4 bits per pixel without significant dependence on position in the FOV or stellar density. In contrast, the K2 B value increased roughly linearly with radial distance from the FOV center (as does roll motion), and as the square root of the number of stars per square degree (n^*) until n^* reached a limit, above which B is insensitive to n^* . Barclay (2016, private communication), following Olbers (1823), conjectured that B stops increasing with n^* since the sky as sampled by *Kepler*'s 4.0 arcsec pixels becomes more uniform, not less, as n^* increases. This “Olbers-Barclay” limit is roughly 1.2×10^4 stars per square degree for EPIC stars with $11.5 < K_p < 14.5$. The maximum contribution of n^* to B is then 5.0 bits per pixel, and the maximum B for K2 data with in-family roll errors is ~ 15 bits per pixel. Hence, it is always beneficial to compress the 16-bit requantized data (steps 2 and 3 described above). In regions of low n^* , such as the Galactic caps, the average B over the FOV is roughly 7.2 bits per pixel after the introduction of the new Huffman table in C5, which is a better match to the distribution of data values in K2.

3.5. Fidelity of World Coordinate System (WCS)

Handberg & Lund (2017) did an independent study of the fidelity of the K2 WCS for both Type-1 and Type-2 TPFs. They found that the absolute correction in pixels to the estimated position of targets, based on the WCS provided in target pixel files, was a function of angular distance to the FOV center (see Figure 6 of Handberg and Lund 2017). For the Type-1 TPFs, with a model-derived WCS, corrections could be as large as 1 pixel, while for Type-2 TPFs (C3 and C4) the maximum correction was 0.5 pixels with typical corrections ~ 0.2 pixels. They conclude, for Type-2 TPFs, “...this level of offset should in general be small enough to correctly identify targets in the frames.” Figure 9 of Lund et al. (2015) shows graphically the correction of the WCS pixel positions in the original (Data Release 2) C0 Type-1 TPFs.

Regarding custom apertures, the TPFs used to observe extended and moving objects (see §2.2 and subsections) also have WCS coordinates. Even though there may not be a well-defined point source in the aperture, a centroid is nonetheless calculated to set the reference location within each aperture (keywords CRPIX1 / CRPIX2). While this position is arbitrary, the WCS transformation is derived from the motion polynomials (Van Cleve 2010), which are calculated from good stars on that channel, not from the custom aperture itself. Thus, the WCS keywords in custom apertures should correctly describe the mapping of pixels to the sky to better than a few pixels.

3.6. Moving Targets

Since the *Kepler* spacecraft observed near the ecliptic during the K2 mission, moving targets, i.e., Solar System Objects (SSOs), frequently crossed the field of view. Users should be aware that when these objects cross other K2 targets, they can cause spurious signals in the stellar photometry — this could be as minor as an asteroid passing through a stellar target's aperture, or as major as a bright solar system planet in the FOV. For example, in C5, Mars affected multiple channels and thousands of targets as it passed through the field of view. However, pointing near the ecliptic also presents an opportunity for K2 to uniquely characterize the light curves of SSOs for long, uninterrupted durations. As described in §2.2.4, K2 targeted many SSOs using tiled masks, in order to extract photometry of solar system objects.

Extracting photometry from K2 observations of SSOs is a complicated endeavor given that SSOs move at different apparent speed (depending on their orbital separation from the Sun and their position in the solar system relative to the Kepler spacecraft), and in some cases move as fast as several pixels during a long-cadence exposure. Also, they are often very bright or very faint, with some comets and asteroids fainter than 20th magnitude, where the precision is ~100,000 ppm (0.1 mag) for a long cadence exposure (Ryan et al. 2017). Nonetheless scientifically useful photometry has been obtained from K2 data for multiple SSOs. For instance, K2 photometry of Neptune has been used to observe solar oscillations (Gaulme et al. 2016) and to compare broad band photometry to known cloud features (Simon et al. 2016). K2 data has been combined with Herschel and Spitzer observations to study the irregular satellites of Uranus (Farkas-Takács et al. 2017). Photometric accuracy sufficient for rotation rate determination was achieved for SSOs as faint as ~22nd magnitude (e.g., Szabó et al. 2017, Molnár et al. 2018, Marton et al. 2020, and Szabó et al. 2020).

3.7. Spurious Frequencies

Kepler and K2 data exhibit spurious frequencies due to a variety of instrumental effects. The K2 data exhibits all the spurious frequencies seen in Kepler data as well as additional spurious frequencies due to the use of regular thruster firings to maintain pointing. Exhaustive investigations of Kepler spurious frequencies have previously been documented and will only be briefly discussed here. The impact of thruster firings on K2 data products is demonstrated.

3.7.1 Spurious Frequencies seen in Kepler Data

The KDCH describes a number of sources of spurious frequencies that may be found in long-cadence and short-cadence Kepler data that could significantly affect scientific analyses (e.g., asteroseismology). The period of long-cadence observations is 29.4244 minutes and the Nyquist frequency is 283.183 μ Hz. Table 5 of the KDCH specifically lists 3 spurious frequencies *below* the LC Nyquist frequency at 86.8, 196.5, and 242.5 μ Hz. Further discussion of these frequencies can be found in Section 5.11.2 of the KDCH. Murphy (2012) warns that one “must exercise extreme caution when analysing LC data if there are no SC data to test for aliasing problems associated with the LC Nyquist frequency.”

Short-cadence observations are usually more affected than long-cadence observations. The systematic-error correction scheme of the Kepler pipeline for *short-cadence* light curves uses the basis vectors and fit coefficients found by Bayesian MAP (Smith et al. 2012, Stumpe et al. 2012, 2014) for the corresponding *long-cadence* light curves (KDCH §5.11). This was due to the fact that there was an insufficient number of short-cadence light curves on any given output channel to adequately form a reasonably complete set of basis vectors which would have allowed MAP to be implemented directly. This “quickMAP” method is described in §8.5.7 of the KDPH.

The period of short-cadence observations is exactly thirty times shorter than the period of long-cadence observations (58.84876 s). A 30:1 spline interpolation of the LC basis vectors to the SC sampling times cannot adequately represent signals in SC observations with frequencies above the Nyquist frequency of LC observations. Consequently, spurious signals in SC observations above 283.2 μ Hz will not be

effectively removed by PDC. The only mitigation available to the user of K2 SC observations consists of identifying common-mode signals and then either 1) removing them or 2) ignoring them (KDCH §5.11).

Gilliland et al. (2010) found the first significant set of spurious frequencies in short-cadence power spectral density distributions in Q1 observations — the fundamental and all harmonics of the inverse of the LC period, n/LC ($= n \cdot 566.391 \mu\text{Hz}$, where n is a positive integer), which is sometimes referred to as the “LC (frequency) comb”. Figure 2 of Gilliland et al. shows that the mean amplitude spectra of samples of quiet stars, and even bright ($K_p = 9$ mag) stars, exhibit this dominant spectral feature from the seventh and eighth harmonics; a variant of that graph, based on Q11 data, is shown in Figure 15 of the KDCH. Although the physical cause of this problem is still not understood, it is presumably related to power and thermal cycles in the *Kepler* photometer electronics (LDE) as events repeat themselves every LC period (KDCH §5.11). These spurious frequencies are not due to an artifact introduced by the Kepler pipeline, since they also appear in raw trailing black collateral data which indicates an additive (not multiplicative) systematic error. These spurious signals were stable in frequency and amplitude throughout the Kepler mission, and are considered to be a normal feature of SC observations (KDCH §5.11).

A list of spurious frequencies found in Kepler short-cadence Q0 to Q14 observations was supplied to the Kepler Mission by Andrzej Baran (see also Baran 2013 and references therein). An updated list of spurious frequencies in SC data was presented in Table 7 of the Kepler Data Release 12 Notes (KSCI-19052-001; November 30, 2011). Table 5 of the KDCH is an updated version of the DRN12 table. Users are advised to check frequency detections in SC observations against this master list of possible spurious SC frequencies (KDCH Table 5). Users are also cautioned to do their own tests to check for the existence of non-astrophysical common-mode signals in Kepler and K2 SC data.

3.7.2 Spurious Frequencies seen in K2 Data

Thruster firings of the *Kepler* spacecraft were rare events during the Kepler mission, but they were routinely used to maintain accurate pointing during K2. These thruster firings are the dominant source of spurious frequencies in K2 observations. As explained in §2.1.2, after every 12th cadence, the spacecraft would autonomously decide if a brief thruster firing was necessary. The imprint of this once per every 5.8849 hour activity exists in K2 data. The resulting spacecraft motion causes the reported flux to vary if targets move into and out of the photometric aperture. In addition, smaller photometric variations result from both inter- and intra-pixel sensitivity variations as the target star moves from pixel to pixel (Vorobiev et al. 2018; Saunders et al. 2019).

The size of the optimal photometric aperture used by the Kepler/K2 pipeline is chosen to maximize the S/N on 6-hour time scales (Smith et al. 2016). During normal K2 operations, target starlight from the wings of the Point-Spread Function will slowly exit the OA, while contaminating light from nearby stars may enter from the other side of the OA. After a position-correction thruster firing, the star returns to the center of its OA, which can result in an abrupt change in flux. The amount of motion across the detector due to spacecraft roll is dependent on the distance of the target from the center field of view. Targets near the edge of a K2 campaign field of view exhibit the largest motion, and therefore have the largest potential for motion-induced flux variations.

The unmistakable signature of thruster firings on K2 photometry can be seen in the top panel of Figure 15. The normalized long-cadence Simple Aperture Photometry (SAP) flux light curve of EPIC 211414081, a $K_p = 12.447$ magnitude star observed in Campaign 5, exhibits the ~6 hour repeating variation that is characteristic of K2 data. This star fell on channel 13 which is near the edge of the FOV.

Several data products result from efforts to detrend K2 lightcurves. The Kepler/K2 PDC pipeline module, as well as several High Level Science Products (e.g., K2SFF, EVEREST, and K2SC; see §4.2.1), all aim to eliminate the signature of thruster firings. In general, each method has its strengths and weaknesses. Users may want to compare the lightcurves available among these data products.

The normalized long-cadence Kepler/K2 pipeline Presearch Data Conditioning Simple Aperture Photometry (PDCSAP) flux light curve of EPIC 211414081 (see middle panel of Figure 15) shows that the PDCSAP processing has successfully reduced the impact of the thruster firings; it is difficult to see in the inset graph where the position-correction thruster firings occurred. Depending on the application, examining the light curve may be insufficient to assess the remaining impact of the thruster firings. For example, the periodogram of the PDCSAP data of EPIC 211414082 (bottom panel of Figure 15) clearly exhibits a peak at 5.846 ± 0.019 hours, which is statistically consistent with the expected 5.8849 hour thruster period.

Short-cadence K2 data also exhibit spurious signals due to the regular thruster firings. The short-cadence SAP lightcurve of EPIC 211414081 (top panel of Figure 16) exhibits the same characteristic signature of K2 thruster firings as was seen in the long-cadence SAP lightcurve (Figure 15). As was the case for Kepler (see §3.7.1), removing spurious frequencies in short-cadence data is significantly harder than removing spurious frequencies from long-cadence data. The PDCSAP light curve of EPIC 211414081 (middle panel of Figure 16) shows that the detrending is incomplete in the immediate vicinity of the thruster firings. There is currently no HLSP that attempts to detrend short-cadence data.

The imprint of the regular thruster firings on the short-cadence data of EPIC 211414081 is easily seen in the frequency space periodogram of both the SAP flux and PDCSAP flux (bottom panel of Figure 16 and Figure 17). The 5.8849 hour period due to thruster firings corresponds to a frequency of 47.1993 μHz . This frequency and its harmonics are clearly seen in both periodograms. While PDC does not eliminate the spurious frequencies due to thruster firing, a comparison of the middle and bottom panels of Figure 17 demonstrate that PDC is effective at eliminating low frequency trends.

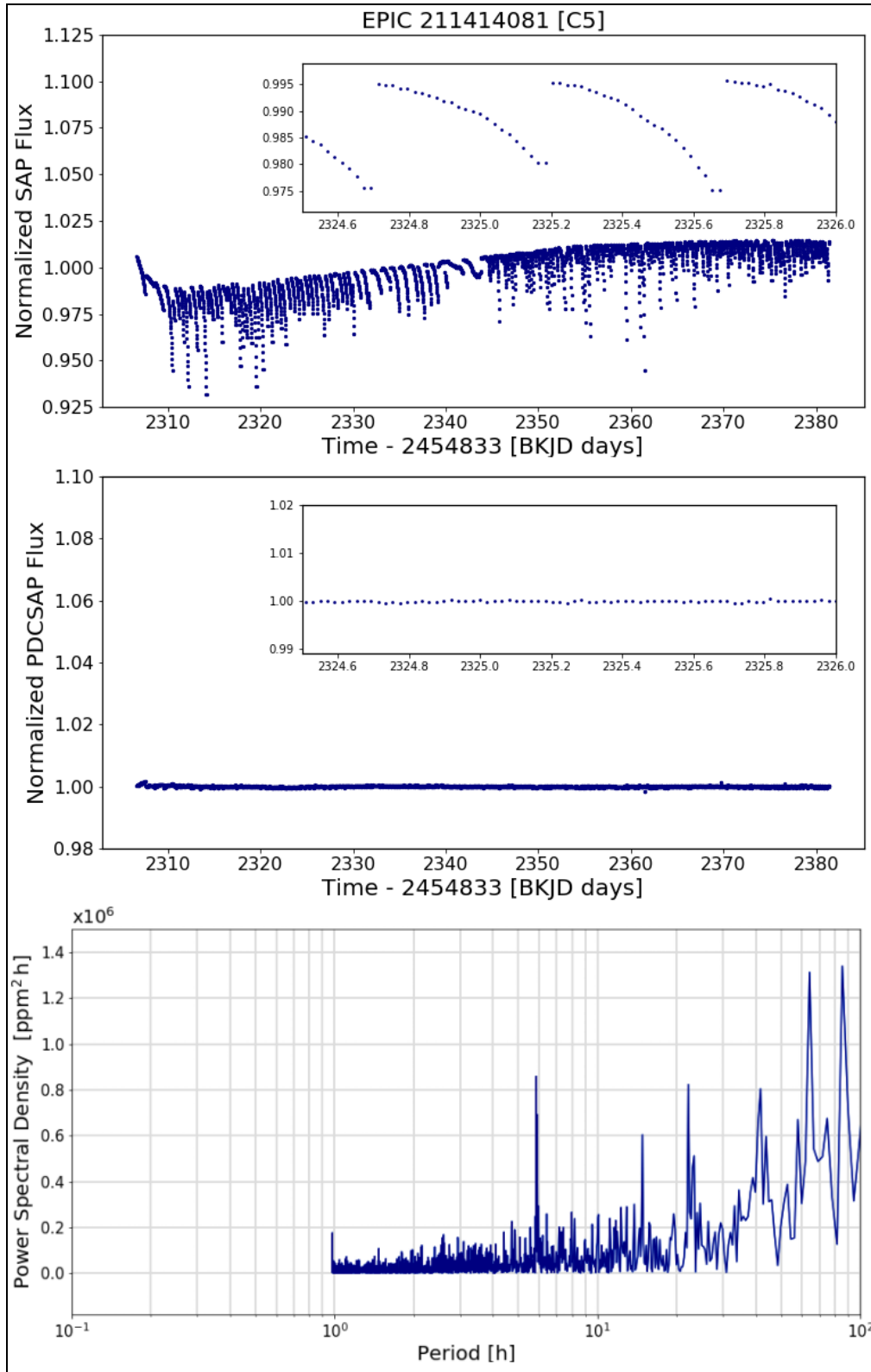


Figure 15: The C5 target EPIC 211414081. Top: The normalized long-cadence SAP flux light curve; inset shows a magnified view of the effect of 3 normal thruster firings. Middle: The normalized long-cadence PDCSAP flux light curve; inset has the same range as the top panel inset. Bottom: The PDCSAP flux periodogram for the high-frequency portion (1–100 hours).

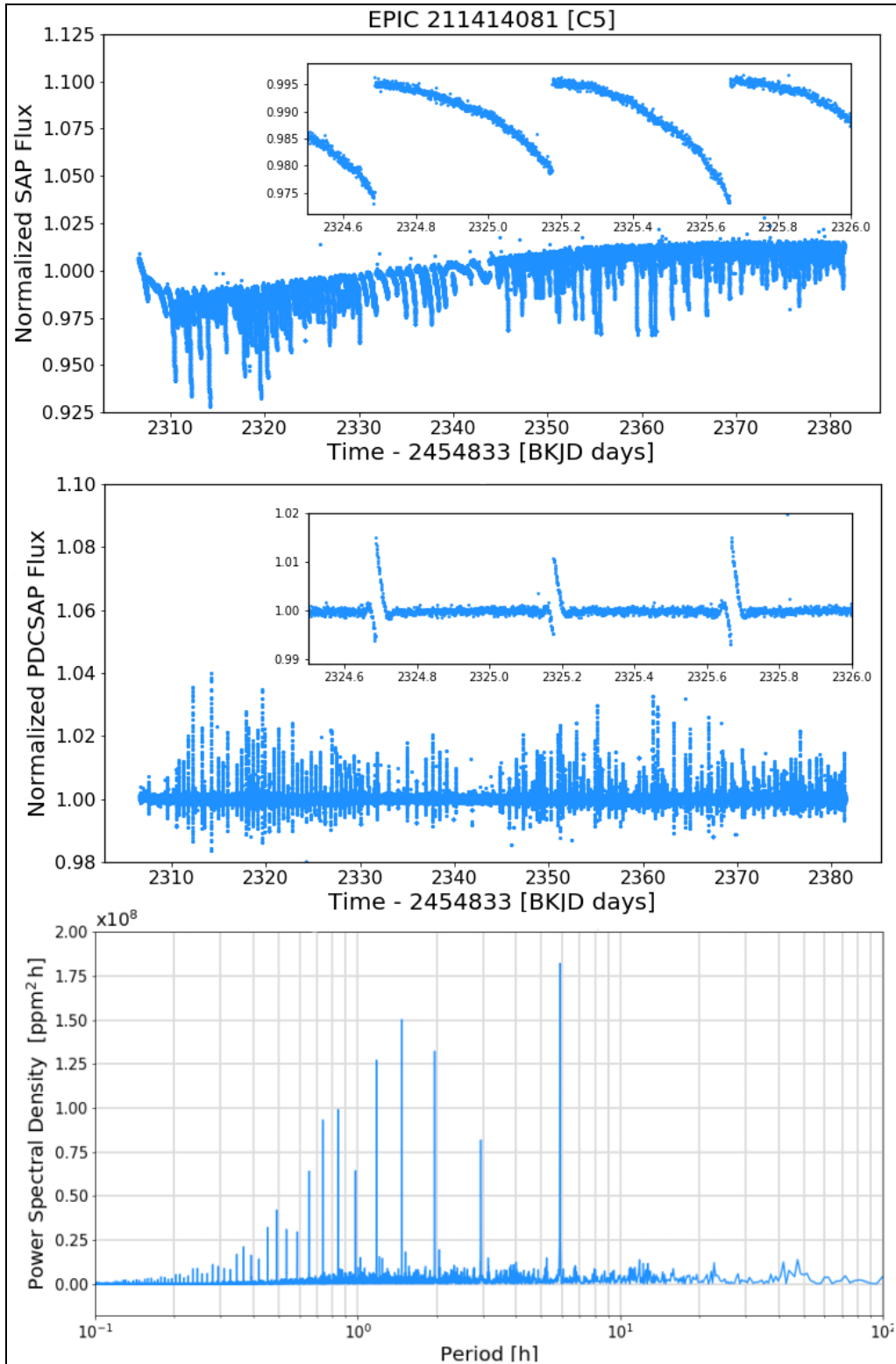


Figure 16: Short-cadence observations of C5 target EPIC 211414081. Top: The normalized SAP flux light curve; inset shows a magnified view of the effect of 3 normal thruster firings. Middle: The normalized PDCSAP flux light curve; inset shows a magnified view of the effect of 3 normal thruster firings. Bottom: The short-cadence PDCSAP flux periodogram. Some of the power peaks (from right to left) occur at about 6, 3, 2, 1.5, and 1 hour.

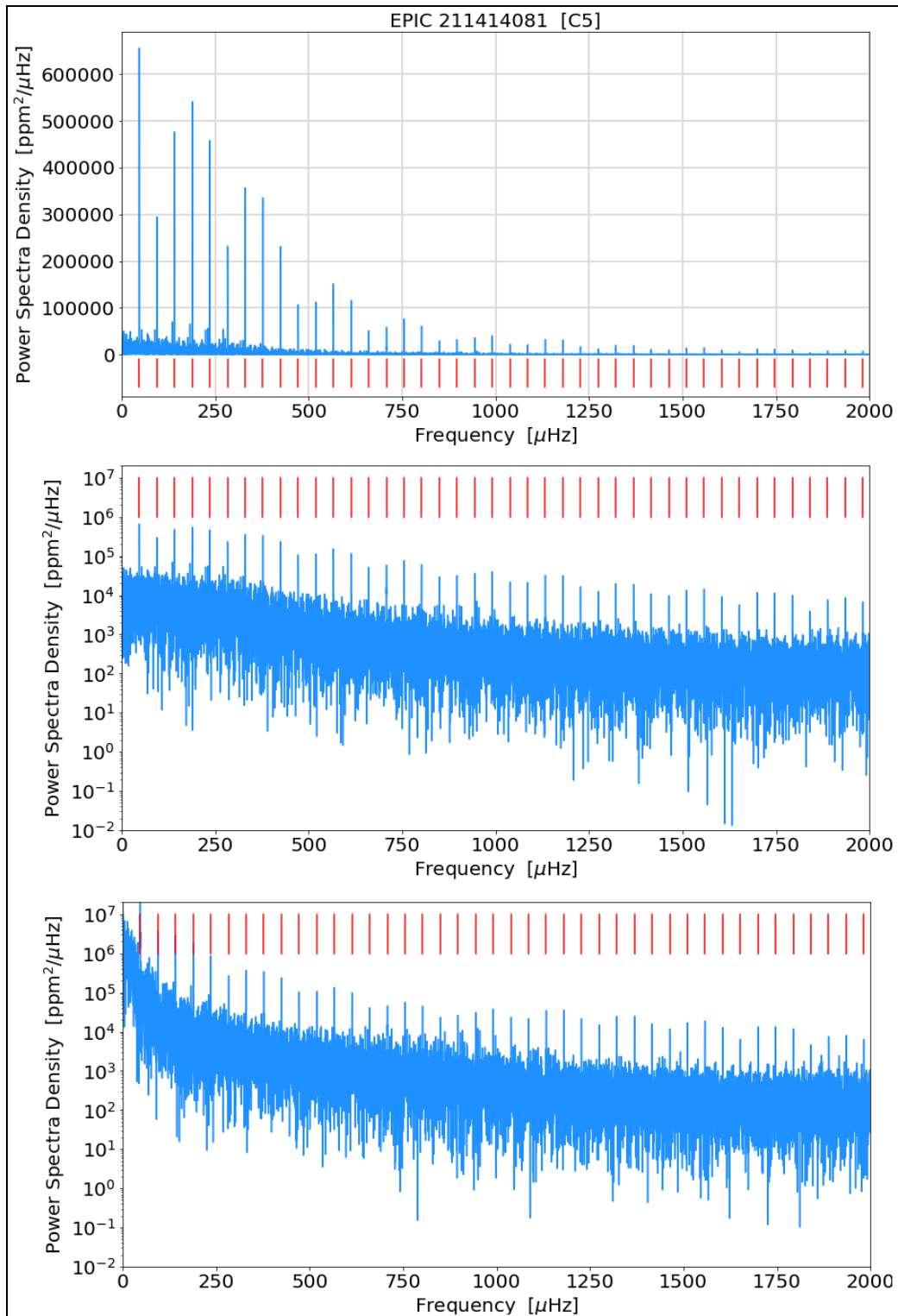


Figure 17: Top and middle panels are short-cadence PDCSAP flux periodograms in the frequency domain with a linear (top) and logarithmic (middle) y-axis for the C5 target EPIC 211414081. The bottom panel is the same as the middle, but based on SAP flux instead of PDCSAP flux; there is more noise (power) at lower frequencies, as expected with non-detrended light curves, and the spurious frequencies caused by the spacecraft motion to restore pointing are similar to those in the PDCSAP flux version. The **red bars** are harmonics of 47.1993 μHz (5.88521 hours).

4. K2 Data Search and Retrieval

The MAST Kepler Archive Manual (Mullally 2020) has information on the Kepler mission files at the public NASA archives. The K2 archive products are very similar to the Kepler data products, but they are not specifically addressed in the MKAM. This section details the K2 data that is available in the NASA archives — the Mikulski Archive for Space Telescopes (MAST) and the NASA Exoplanet Science Institute (NExSci) archive. For clarity the datasets are described in two separate categories: those produced by the mission, and those produced by the scientific community.

4.1. Mission-Produced Data

The MAST hosts all of the mission-produced K2 data (<http://dx.doi.org/10.17909/t9-6zdf-eh42>). The MAST K2 website describes the data products and provides several options and tools for users to search and retrieve K2 data. Questions about accessing the MAST archive for K2 archive data products should be emailed to the MAST Help Desk at STScI (archive@stsci.edu).

4.1.1 The Ecliptic Planet Input Catalog (EPIC)

The K2 EPIC (more than 50 million rows) provides EPIC IDs and associated information (e.g., positions, magnitudes, etc.) for Campaigns 0–19, as described by the EPIC doc (Huber & Bryson 2019; KSCI-19082-21). Stellar information (temperatures, surface gravities, metallicities, radii, masses, densities, distances, and extinctions) for IDs corresponding to standard apertures in C0–C8 and C10–C19 is also included. No stellar parameters are included for C9 due to difficulties related to the field's extreme stellar density. The EPIC can be searched via a website interface or directly downloaded from MAST.

4.1.2 Raw Cadence Data

The raw cadence data as downloaded from the spacecraft is available for every K2 campaign. Users should read KADN-26315 (Haas 2015), available at the K2 Documentation page at MAST, for a description of the format. The *Kadenza* software tool (Barentsen & Cardoso 2018) can be used to convert the raw data into more traditional multi-extension image FITS files.

4.1.3 Calibration Files

The following files are used in the calibration of the target pixel and light curve files and are available at MAST. They are each described in the MAST Kepler Archive Manual, with the corresponding section number given in parentheses.

- SPICE kernels used to calculate the Kepler spacecraft ephemeris (See MKAM §2.1.2)
- Cotrending Basis Vector (CBV) files (See MKAM §2.3.4)
- Background Pixel (BKG) files (See MKAM §2.3.6)
- Long and Short Cadence Collateral (COLL & COLS) files (See MKAM §2.3.7)
- Artifact Removal Pixel (ARP) files (See MKAM §2.3.8)
- Thruster firing flag data for C9 and C10a (See §2.4 and MKAM Table 2-3; note only used for K2)

4.1.4 Target Pixel and Light Curve Files

The target pixel and light curve files for all successfully processed targets for each campaign are retrievable via a website search interface and direct download at MAST. These include:

- Long-cadence light curve files (`ktwo2*_llc.fits`)
- Short-cadence light curve files (`ktwo2*_slc.fits`)
- Long-cadence target pixel files (`ktwo2*_lpd.fits`)
- Short-cadence target pixel files (`ktwo2*_spd.fits`)

4.1.5 Full Frame Images

Full Frame Images (FFIs; also sometimes referred to as Full Field images) are 30-minute exposures of all active CCDs, including both real and virtual pixels. Nominally there were 2 FFIs collected per K2 campaign. The number of FFIs collected can be found in Table 4. Three FFIs were collected for C0 for enhanced diagnostics in this inaugural campaign. Only one FFI was collected in campaigns 13 and 15 in order to leave enough storage space for the target cadence data. Due to indications that the spacecraft fuel tank was running very low ~50 days into C18, the collection of science data for C18 was terminated on July 2, 2018 and the spacecraft was put into hibernation until the data was downloaded at the regularly scheduled time in early August. As a result, only one FFI was collected in C18. Overall, 38 FFIs were collected during the K2 mission.

The 38 calibrated K2 FFIs are available at MAST (<http://dx.doi.org/10.17909/t9-md34-7k30>), with a full list provided below. The file names show the integration stop time in [year][3 digit day of year][hhmmss] format, followed by the campaign number. The FFIs have the same integration parameters as an LC exposure (~29.4 min), as was the case during the Kepler mission. The K2 mission has produced grayscale PNG versions of entire FFIs, individual modules, and individual channels that are available at MAST (<http://dx.doi.org/10.17909/t9-w7y2-yf63>). The compass rose seen in the FFI PNG images uses the optical astronomy convention of having the end of the long compass rose arm to point North (increasing declination) and the end of the short compass rose arm to point East (increasing right ascension).

```
ktwo2014070234206-c00_ffi-cal.fits
ktwo2014074233223-c00_ffi-cal.fits
ktwo2014110010101-c00_ffi-cal.fits
ktwo2014157010055-c01_ffi-cal.fits
ktwo2014203150825-c01_ffi-cal.fits
ktwo2014240042843-c02_ffi-cal.fits
ktwo2014294030900-c02_ffi-cal.fits
ktwo2014331202630-c03_ffi-cal.fits
ktwo2015008010551-c03_ffi-cal.fits
ktwo2015051131033-c04_ffi-cal.fits
ktwo2015092174954-c04_ffi-cal.fits
ktwo2015127093352-c05_ffi-cal.fits
ktwo2015170131810-c05_ffi-cal.fits
ktwo2015207050529-c06_ffi-cal.fits
ktwo2015246104018-c06_ffi-cal.fits
ktwo2015290001304-c07_ffi-cal.fits
ktwo2015331045232-c07_ffi-cal.fits
ktwo2016014203204-c08_ffi-cal.fits
ktwo2016056011138-c08_ffi-cal.fits
ktwo2016119231109-c91_ffi-cal.fits
ktwo2016153221424-c92_ffi-cal.fits
ktwo2016199030108-c102_ffi-cal.fits
ktwo2016240074042-c102_ffi-cal.fits
ktwo2016279022810-c111_ffi-cal.fits
ktwo2016307123729-c112_ffi-cal.fits
ktwo2016361035629-c12_ffi-cal.fits
ktwo2017032102633-c12_ffi-cal.fits
ktwo2017079075530-c13_ffi-cal.fits
ktwo2017162122209-c14_ffi-cal.fits
ktwo2017203170143-c14_ffi-cal.fits
ktwo2017246053350-c15_ffi-cal.fits
ktwo2017344214411-c16_ffi-cal.fits
ktwo2018030100110-c16_ffi-cal.fits
ktwo2018073065336-c17_ffi-cal.fits
ktwo2018112122825-c17_ffi-cal.fits
ktwo2018143080022-c18_ffi-cal.fits
ktwo2018249002316-c19_ffi-cal.fits
ktwo2018268151041-c19_ffi-cal.fits
```

4.1.6 Engineering Data for Science Campaigns

Ancillary engineering data (AED) are available at MAST for Kepler and K2 (KIH §2.5; MKAM §2.3.10 and Appendix B.5). The Kepler and K2 AED files can be retrieved, respectively, at these two MAST websites: <http://dx.doi.org/10.17909/t9-2w9p-7e82> and <http://dx.doi.org/10.17909/t9-pr3a-mf61>. The names of the AED files and their contents are described in the K2 document Mighell & Van Cleve (2020; KSCI-19150-001). Telemetry data of particular interest to K2 users are those which measure quantities and systems that behaved differently during the K2 mission, such as the mean roll angle error (ADATTERRMX) and the various temperatures of subsystems which experienced a different thermal environment during the K2 mission than in the Kepler mission (Mighell & Van Cleve 2020; KSCI-19150-001). Figure 18 shows an example of the *Kepler* spacecraft roll errors due to the slow roll motion caused by solar radiation pressure.

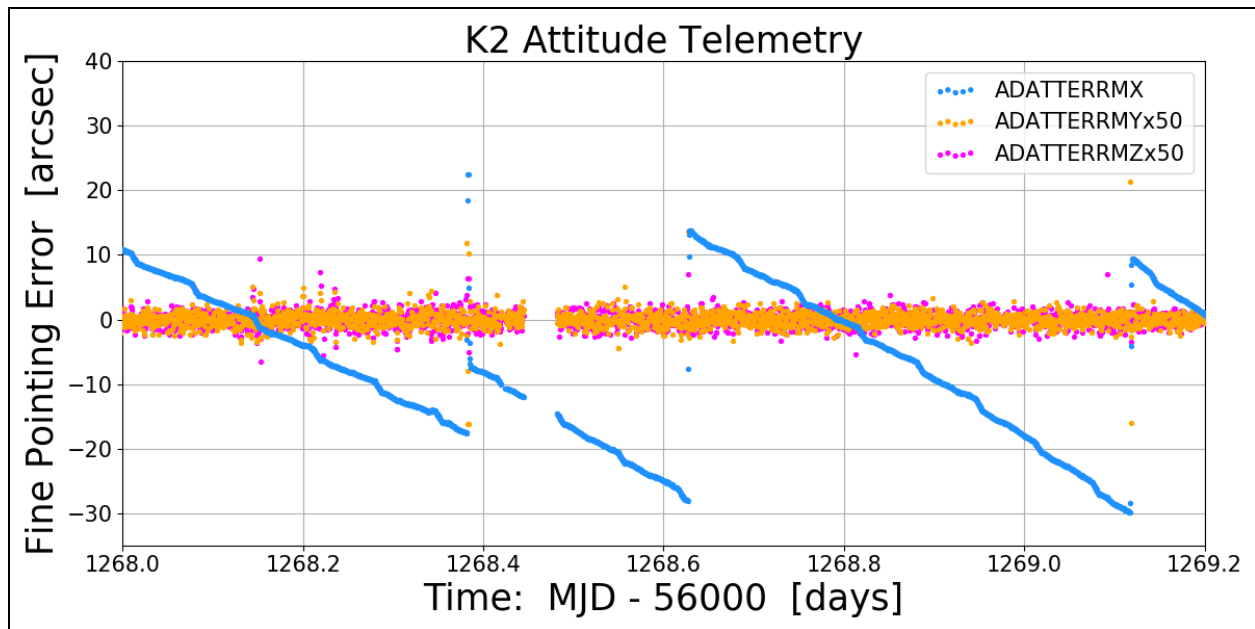


Figure 18: Example Engineering Telemetry from K2. ADATTERRMX is the mean fine-pointing rotation-angle error about the boresight. All three fine-pointing rotation-angle error means (ADATTERRMX, ADATTERRMX, and ADATTERRMZ) were converted from radians to arcseconds (arcsec). The plotted values for ADATTERRMX and ADATTERRMZ have been multiplied by 50 in order to show a magnified view of the data. The large excursions in ADATTERRMX were caused by brief commanded thruster firings used to maintain pointing accuracy of the *Kepler* spacecraft.

4.1.7 FGS Data for Science Investigations

The FGS data are available at MAST for science investigations for the Kepler mission (<http://dx.doi.org/10.17909/t9-pwsq-fb48>) and the K2 mission (<http://dx.doi.org/10.17909/t9-49ap-p353>) in the form of centroid/flux time series and as (relatively infrequent) FGS FFIs. These data contain the highest time sampling possible with *Kepler*, with integration times of 0.104 seconds. Users may find them useful for studying stellar variability or eclipsing binaries (e.g., the C6 guide star was found to be a ~0.6 day contact binary), or use the FGS data to more fully understand pointing effects on the science data. More information is available in the document KSCI-19112-002 (Mighell & Van Cleve 2019).

4.1.8 Two-Wheel Concept Engineering Test Data (E2)

The year-long transition from Kepler to K2 following the reaction wheel failures is detailed in Larson et al. (2014). Part of this transition was a 9-day engineering test (E2) conducted before Campaign 0. While E2 was not intended for science, the data have been made available as uncalibrated TPFs at MAST: <http://dx.doi.org/10.17909/t9-3gvt-3w97>. The E2 FOV overlaps with C12 to a large extent, so users might do their own reduction of E2 data for comparison to C12 observations to look for long-term trends in common objects. The E2 FOV was centered at (RA, DEC) = (358.5, -2.4). The filenames at MAST use non-standard Kepler IDs between 60017806 and 60044117; *they are not in the EPIC*, so users will have to match the RA and DEC to some other suitable catalog.

4.1.9 Driftscan FFI

Driftscanning was an experimental data collection mode during which the telescope collected an FFI while the telescope was drifting. A short pilot program was carried out on May 10–11, 2018 to evaluate the feasibility of this mode. Five driftscan FFIs were collected during the K2 Campaign 17 (C17) Deep Space Network (DSN) downlink, after all C17 science data had been safely telemetered and spare DSN time remained. These five raw FFIs are available at MAST — the FFIs were never calibrated by the Kepler/K2 pipeline.

Driftscanning produces long overlapping star-trails on the FFI, rather than conventional stationary point-sources. The expected length of the startrails is ~270 pixels based on an anticipated spacecraft drift motion of ~0.5 degrees per hour — the actual rate of spacecraft motion has not been measured. The direction of pointing of the telescope is not known a-priori, but can in principle be derived from the distinct constellation pattern of star trails.

The driftscan FFIs were acquired with the same combined exposure time as conventional 30-minute long cadence FFIs, i.e., 270 onboard-coadded integrations with 6.02s exposure time and 0.52s readout time per integration. The images were acquired sequentially with gaps ranging from 30 minutes to 4 hours.

A potential use of the driftscan FFIs would be to enhance the flat-field calibration of the *Kepler* focal plane, since the relative response of adjacent pixels can be derived from the apparent variations in pixel flux as the same point spread function moved across the focal plane. Note that the detector electronics may have additional noise arising from radio frequency interference during the DSN contact.

The five driftscan FFIs are available at MAST: <http://dx.doi.org/10.17909/t9-tpjj-hm05>. The filenames of the driftscan FFIs are:

- kplr2018131024020_ffl-orig.fits
- kplr2018131032646_ffl-orig.fits
- kplr2018131041344_ffl-orig.fits
- kplr2018131094047_ffl-orig.fits
- kplr2018131130639_ffl-orig.fits

4.1.10 NExSci K2 Targets Table

The NExSci K2 Targets Table (see <https://exoplanetarchive.ipac.caltech.edu/docs/K2Mission.html>) lists astrometric, photometric, stellar, and other information for observed targets. The table allows users to download mission-produced light curve FITS files that are hosted at NExSci, as well as .tbl text files produced by NExSci based on the FITS files. Users are cautioned that at the time of this writing not all data releases are hosted at NExSci. As a result, light curve files for some campaigns may not be from the most recent processing. Users should also note this table is likely to be updated not long after the publication of this document, though the exact timeframe is uncertain.

4.2. Community-Based K2 Science Products

Numerous data products have been produced for and/or by the scientific community and made publicly available at the NASA archives. Below is a listing and description of these products.

4.2.1 MAST HLSPs

Besides the mission-produced K2 data products at MAST already described above, MAST also hosts community-created High Level Science Products (HLSPs), which are observations, catalogs, or models that complement, or are derived from, MAST-supported missions. HLSPs for the K2 mission can be found by going to the MAST HLSP website (<http://dx.doi.org/10.17909/t9-8ncg-g847>) and selecting the K2 option of the “Mission” pull-down menu, then clicking the “SUBMIT” button.

MAST currently has the following High Level Science Products for the K2 mission:

- **K2SFF**: K2 Extracted Light Curves [PI: Vanderburg, A.]
- **EVEREST**: EPIC Variability Extraction & Removal for Exoplanet Science Targets [PI: Luger, R.]
- **HALO**: The K2 Bright Star Survey [PI: Pope, B.]
- **K2SNE**: PanSTARRS Follow-up of K2 Campaign 16 and 17 Supernova Fields [PI: Dotson, J. L.]
- **KEGS**: Kepler Extra-Galactic Survey [PI: Shaya, E.]
- **K2GAP**: K2 Galactic Archeology Program [PI: Stello, D.]
- **POLAR**: K2 Extracted Light Curves [PI: Barros, S.]
- **K2SC**: K2 Systematics Correction [PI: Aigrain, S.]
- **K2VARCAT**: K2 Variability Catalog [PI: Armstrong, D. J.]
- **K2SUPERSTAMP**: Astrometrically Calibrated Images of Cluster Regions Observed by K2 [PI: Cody, A. M.]

4.2.2 NExSci Data Tables

NExSci has the following community-based products that it created and maintains to support the K2 mission (see <https://exoplanetarchive.ipac.caltech.edu/docs/K2Mission.html>). Questions about accessing these data products should be emailed to the NExSci Help Desk (exofop-support@ipac.caltech.edu).

4.2.2.1 K2 Candidates Table

The K2 Candidates table is a table of published K2 candidate exoplanets and their associated parameters, as compiled by NExSci. The table is accessible manually using the above website or automatically using the K2 Applications Programming Interface (API) described at https://exoplanetarchive.ipac.caltech.edu/docs/program_interfaces.html#k2.

4.2.2.2 K2 Names Table

The K2 Names table maps EPIC numbers to named K2 exoplanets, as compiled by NExSci. All of these planets were identified and confirmed by the community. The table is accessible manually using the above main NExSci website or programmatically using the K2 API given above.

4.2.2.3 K2 ExoFOP

NExSci currently hosts the Exoplanet Follow-up Observing Program for K2 website (ExoFOP-K2) at <https://exofop.ipac.caltech.edu>. The website has stellar parameters (if available) from the EPIC, finder charts, and information on nearby sources for objects observed by K2. ExoFOP-K2 also serves as a repository for community-gathered follow-up data. Links to a variety of analysis tools are provided. All data on ExoFOP-K2 is public. The website is open to the entire community and all content can be viewed and downloaded without logging in. A username and password are only required in order to upload data, notes, and/or files.

References

Key Websites

<http://dx.doi.org/10.17909/t9-wkvz-3437> (MAST-Kepler)

<http://dx.doi.org/10.17909/t9-97cz-d806> (MAST-K2)

Publications (Note: DOIs are provided for AIAA papers to make them more easily accessible.)

- Baran, A. S. 2013, *Acta Astronomica*, 63, 203
- Barentsen, G. & Cardoso, J. V. de M. 2018, *Kadenza*, ascl:1803.005
- Bryson, S. T., et al. 2010a, *ApJL*, 713, L97
- Bryson, S. T., Jenkins, J. M., Klaus, T. C. et al. 2010b, *Proc. SPIE*, Vol. 7740, 77401D
- Christiansen, J. L., Jenkins, J. M., Caldwell, D. A., et al. 2012, *PASP*, 124, 1279
- Chaplin, W. J., & Miglio, A. 2013, *ARAA*, 51, 353
- Cody, A. M., Barentsen, G., Hedges, C., et al. 2018a, *RNAAS*, 2, 25
- Cody, A. M., Barentsen, G., Hedges, C., et al. 2018b, *RNAAS*, 2, 199
- Farkas-Takács, A., Kiss, C., Pál, A., et al. 2017, *AJ*, 154, 119
- Gaulme, P., Rowe, J. F., Bedding, T. R., et al. 2016, *ApJL*, 833, L13
- Gilliland, R. L., Jenkins, J. M., Borucki, W. J., et al. 2010, *ApJ*, 713, L160
- Handberg, R., & Lund, M. N. 2017, *A&A*, 597, A36
- Howell, S. B., Sobeck, C., Haas, M. R., et al. 2014, *PASP*, 126, 398
- Huber, D., Bryson, S. T., Haas, M. R., et al. 2016, *ApJ Supplement*, 224, 2
- Jenkins, J. M., Dunnuck, J. 2011, *Proc. SPIE Vol. 8146*, 814602
- Larson, K. A., McCalmont, K. M., Peterson, C. A., & Ross, S. E. 2014, *SpaceOps 2014 Conference, SpaceOps Conferences, (AIAA 2014-1882)* <http://dx.doi.org/10.2514/6.2014-1882>
- Lund, M. N., Handberg, R., Davies, G. R., Chaplin, W. J., Jones, C. D. 2015, *ApJ*, 806, 30L
- Marton, G., Kiss, C., Molnár, L., et al. 2020, *Icarus*, 345, 113721
- McCalmont, K. M., Larson, K. A., Peterson, C. A., & Ross, S. E. 2015, *AIAA SPACE 2015 Conference and Exposition*, doi: 10.2514/6.2015-4530
- Molnár, L., Pál, A., Sárneczky, K., et al. 2018, *ApJS*, 234, 37
- Mullally, S. 2020, "MAST Kepler Archive Manual" (MKAM)
- Murphy, S. J. 2012, *MNRAS*, 422, 665
- Olbers, H. W. M. 1823, "ber die Dursichtigkeit des Weltraumes", in *Astronomisches Jahrbuch für das Jahr 1826*, ed. Bodr, J. E. (Berlin: Späten)
- Peterson, C. A., Larson, K. A., McCalmont, K. M., and Ross, S. E. 2015, *AIAA SPACE 2015 Conference and Exposition*, <http://arc.aiaa.org/doi/abs/10.2514/6.2015-4534>
- Pope, B. J. S., White, T. R., Huber, D., et al. 2016, *MNRAS*, 455, L36
- Pope, B. J. S., White, T. R., Farr, W. M., et al. 2019, *ApJS*, 245, 8
- Putnam, D., & Wiemer, W. 2014, *Advances in Astronautical Sciences*, 151, 605
- Putnam, D., Gravseth, I., & Wiemer, D. 2106, *AIAA Guidance, Navigation, and Control Conference (2016)* <http://dx.doi.org/10.2514/6.2016-0366>
- Ryan, E. L., Sharkey, B. N. L., & Woodward, C. E. 2017, *AJ*, 153, 116
- Rubincam, D. 2000, *Icarus*, 148, 2–11
- Saunders, N., Luger, R., & Barnes, R. 2019, *AJ*, 157, 197
- Simon, A. A., Rowe, J. F., Gaulme, P., et al. 2016, *ApJ*, 817, 162
- Smith, J. C., Stumpe, M. C., Van Cleve, J. E., et al. 2012, *PASP*, 124, 1000
- Smith, J. C., Morris, R. L., Jenkins, J. M., et al. 2016, *PASP*, 128:124501
- Stumpe, M. C., Smith, J. C., Van Cleve, J. E., et al. 2012, *PASP*, 124, 985
- Stumpe, M. C., Smith, J. C., Catanzarite, J. H., et al. 2014, *PASP*, 126, 100
- Szabó, G. M., Pál, A., Kiss, C., et al. 2017, *A&A*, 599, A44
- Szabó, G. M., Kiss, C., Szakáts, R., et al. 2020, *ApJS*, 247, 34
- Van Cleve, J. E., Howell, S. B., Smith, J. C., et al. 2016, *PASP*, 128, 075002
- Vanderburg, A., & Johnson, J. A. 2014, *PASP*, 126, 948
- Vorobiev, D., Ninkov, Z., Caldwell, D., et al. 2018, *Proc. SPIE*, Vol.10698, 106985J

Kepler and K2 Mission documents available at MAST

K2 documents: <http://dx.doi.org/10.17909/t9-2btd-va80>

Kepler documents: <http://dx.doi.org/10.17909/t9-n9fp-gs62>

Haas 2015, KADN-26315, "Format Information for Cadence Pixel Files"

Huber, D., & Bryson, S. T. 2019, KSCI-19082-021, "K2: Extending *Kepler*'s Power to the Ecliptic" (EPIC doc)

Jenkins, J. M., et al. 2020, KSCI-19081-003 "Kepler Data Processing Handbook" (KDPH)

Van Cleve, J. E. 2008, KADN-26205, "Selection of LDE Artifact Removal Pixels for Science Operations and Reverse-Clock Calibration"

Van Cleve, J. E. 2010, KADN-26285, "World Coordinate System for Target Pixel FITS Files Derived from Linearized Pipeline Motion Polynomials"

Van Cleve, J. E., & Caldwell, D. A. 2016, KSCI-19033-002, "Kepler Instrument Handbook" (KIH)

Van Cleve, J. E. et al. 2016, KSCI-19040-005, "Kepler Data Characteristics Handbook" (KDCH)

Mighell, K. J., & Van Cleve, J. E. 2019, KSCI-19112-002, "Fine Guidance Sensor Data"

Mighell, K. J., & Van Cleve, J. E. 2020, KSCI-19150-001, "Kepler & K2 Ancillary Engineering Data for Science Data Analysis: Pointing Telemetry, Reaction Wheel Speeds, and Temperatures"

Mullally, S. 2000, "MAST Kepler Archive Manual" (MKAM)

Appendix A. List of Acronyms

AED	Ancillary Engineering Data
AU	Astronomical Unit
ADCS	Attitude Determination and Control Subsystem
API	Applications Programming Interface
ARP	Artifact Removal Pixel
BKJD	Barycentric Kepler Julian Date
CAF	Custom Aperture File
CAL	Calibration (pipeline software)
CBV	Cotrending Basis Vector
CCD	Charge Coupled Device
CDPP	Combined Differential Photometric Precision
COA	Create Optimal Aperture (pipeline module)
CR	Cosmic Ray
DEC	Declination
DOI	Digital Object Identifier
DRN	Data Release Note
EPIC	Ecliptic Plane Input Catalog
FITS	Flexible Image Transport System (digital file format)
FFI	Full Frame Image (a.k.a. Full Field Image in the KIH)
FGS	Fine Guidance Sensor
FOV	Field of View
FWHM	Full Width at Half Maximum
GO	Guest Observer
HLSP	High Level Science Product
http	HyperText Transfer Protocol
https	HyperText Transfer Protocol Secure
ID	Identifier (integer identification number)
JD	Julian Date
JPL	Jet Propulsion Laboratory
K2H	K2 Handbook
KIH	Kepler Instrument Handbook
KDCH	Kepler Data Characteristics Handbook
KDPH	Kepler Data Processing Handbook
KIC	Kepler Input Catalog
LC	Long Cadence
LDE	Local Detector Electronics
LGA	Low Gain Antenna
MAR	Maximum Attitude Residual
MAST	Mikulski Archive for Space Telescopes
MJD	Modified Julian Date = JD - 2400000.5
MKAM	MAST Kepler Archive Manual
NExSci	NASA Exoplanet Science Institute
OA	Optimal Aperture
PA	Photometric Analysis (pipeline software)
PAD	Photometer Attitude Determination (pipeline software)
PDC	Pre-search Data Conditioning (pipeline software)
PDCSAP	Pre-search Data Conditioning Simple Aperture Photometry
PDF	Portable Document Format (document file format)
PNG	Portable Network Graphics (image file format)
PPA	Photometer Performance Assessment (pipeline software)
ppm	parts per million
PRF	Pixel-Response Function

PMRF	Pixel Mapping Reference File
PSD	Power Spectral Density
PSF	Point-Spread Function
RA	Right Ascension
RC	Reverse-Clock (pixels)
SAP	Simple Aperture Photometry
SC	Short Cadence
SCC	Short Cadence collateral
SSO	Solar System Object
SSR	Solid-State Recorder
STScI	Space Telescope Science Institute
TAD	Target and Aperture Definition
TLIF	Target List Input File
TNO	Trans-Neptunian Object
TPF	Target Pixel File
URL	Universal Resource Locator
WCS	World Coordinate System
YORP	Yarkovsky-O'Keefe-Radzievskii-Paddack (effect)